Reciprocal Priming between Receptor Tyrosine Kinases at Recycling Endosomes Orchestrates Cellular Signalling Outputs

Michael P. Smith[1#], Harriet R. Ferguson[1#], Jennifer Ferguson[1], Egor Zindy[2,3], Katarzyna M. Kowalczyk[1,3], Thomas Kedward[4], Christian Bates[1], Joseph Parsons[4], Joanne Watson[5], Sarah Chandler[1], Paul Fullwood[1], Stacey Warwood[6], David Knight[6], Robert B. Clarke[4,7], Chiara Francavilla[1,7,*]

[1]Division of Molecular and Cellular Function, School of Biological Science, Faculty of Biology Medicine and Health (FBMH), The University of Manchester, M139PT, Manchester, UK

[2]Division of Cell Matrix and Regenerative Medicine, School of Biological Science, FBMH, The University of Manchester, M139PT, Manchester, UK.

[3]Present addresses:

EZ: Center for Microscopy and Molecular Imaging, Université Libre de Bruxelles (ULB), CPI 305/1, Rue Adrienne Bolland, 8, 6041 Gosselies, Belgium

KMK: Department of Biochemistry, University of Oxford, OX1 3QU, Oxford, UK

[4]Division of Cancer Sciences, School of Medical Science, FBMH, The University of Manchester, M13 9PT, Manchester, UK

[5]Division of Evolution and Genomic Sciences, School of Biological Science, FBMH, The University of Manchester, M139PT, Manchester, UK

[6]Bio-MS Core Research Facility, FBMH, The University of Manchester, M139PT, Manchester, UK

[7]Manchester Breast Centre, Manchester Cancer Research Centre

#These authors contributed equally

*Lead contact, correspondence: chiara.francavilla@manchester.ac.uk

KEYWORDS

Receptor Tyrosine Kinases (RTKs), Fibroblast Growth Factor Receptor (FGFR), trafficking, signalling, quantitative phosphoproteomics

SUMMARY

Integration of signalling downstream of individual receptor tyrosine kinases (RTKs) is crucial to fine tune cellular homeostasis during development and in pathological conditions, including breast cancer. However, how signalling integration is regulated and whether the endocytic fate of single receptors controls such signalling integration remains poorly elucidated. Combining quantitative phosphoproteomics and targeted assays, we generated a detailed picture of recycling-dependent fibroblast growth factor (FGF) signalling in breast cancer cells, with a focus on distinct FGF receptors (FGFRs). We discovered reciprocal priming between FGFRs and epidermal growth factor (EGF) receptor (EGFR) that is coordinated at recycling endosomes. FGFR recycling ligands induce EGFR phosphorylation on threonine 693. This phosphorylation event alters both FGFR and EGFR trafficking and primes FGFR-mediated proliferation but not cell invasion. In turn, FGFR signalling primes EGF-mediated outputs via EGFR threonine 693 phosphorylation. This reciprocal priming between distinct families of RTKs from recycling endosomes exemplifies a novel signalling integration hub where recycling endosomes orchestrate cellular behaviour. Therefore, targeting reciprocal priming over individual receptors may improve personalized therapies in breast and other cancers.

INTRODUCTION

Receptor tyrosine kinases (RTKs), such as fibroblast growth factor (FGF) and epidermal growth factor (EGF) receptors, respond to perturbations in the environment by initiating signalling cascades in proximity to the plasma membrane upon binding of their growth factors (Wintheiser & Silberstein, 2020). Ligand-induced proximal or early signalling is then amplified through cascades - like the mitogen-activated protein kinase (ERK, p38), phosphoinositide 3-kinase (PI3K), and phospholipase Cγ (PLCγ) pathways - specifies cell fate, and controls cellular homeostasis during development and in pathological conditions (Lemmon & Schlessinger, 2010). Indeed, deregulated early signalling and signalling rewiring are responsible for unwanted long-term outputs, such as increased proliferation and motility, in human diseases, including cancer (Du & Lovly, 2018). This is the main reason why signalling molecules are the target of most of the known cancer therapies (Yaffe, 2019). However, each RTK is not an isolated entity on the plasma membrane, but functions within complex networks with other RTKs to fine tune cancer cell intracellular signalling and long-term fate decisions. Indeed, targeting single molecules is often not enough to switch off unwanted cancer cell responses, as highlighted for instance in breast cancer (Harbeck *et al*, 2019). Recent advances in mass Spectrometry (MS)-based phosphoproteomics allows us to simultaneously analyse thousands of signalling molecules and their post-translational modifications (PTMs) (Bludau & Aebersold, 2020; Doll *et al*, 2019; Huang, 2012; Lundby *et al*, 2019). However, how different RTK families integrate their downstream signalling has not been comprehensively analysed yet. A better understanding of the molecular mechanisms used by RTKs to coordinate each other's signalling architecture will help to identify how to interfere with the right target at the right time to re-direct deregulated cancer cell behaviours. This idea would also support the current therapeutic concept in breast cancer aiming at personalized combination of therapies at early stage of treatment prior to the acquisition of resistance or to delay it (Harbeck *et al.*, 2019).

Multiple mechanisms contribute to shape signalling architecture, including the nature and affinity of the receptor ligand (Zinkle & Mohammadi, 2019), receptor co-activation (Tan *et al*, 2017), feedback mechanisms (Nguyen & Kholodenko, 2016), and the spatio-temporal distribution of signalling transducers (Bergeron *et al*, 2016). Ligand-dependent endocytic trafficking (hereafter trafficking) of RTKs from and to the plasma membrane regulates early signalling and downstream responses (Budick-Harmelin & Miaczynska, 2018; Goh & Sorkin, 2013; Schmid, 2017). For instance, we have shown that fibroblast growth factor 10 (FGF10) and transforming growth factor α (TGFα) initiate specific early signalling events that regulate FGFR2b and EGFR recycling to the plasma membrane, respectively, resulting in enhanced cell motility (Francavilla *et al*, 2016; Francavilla *et al*, 2013). It is however unknown whether ligand-induced recycling plays a role in the signalling interplay between RTKs to coordinate long-term responses. This concept is supported by alterations in the ability of cancer cells to migrate and proliferate due to derailed RTK trafficking (Lanzetti & Di Fiore, 2017; Mellman & Yarden, 2013) and by EGFR/integrin recycling-dependent regulation of cancer cell migration (Caswell & Norman, 2008).

Here, to study how ligand-induced trafficking - and more specifically recycling to the plasma membrane - affected signalling coordination downstream from FGFRs in breast cancer cells we combined

quantitative phosphoproteomics and targeted assays. FGFRs are a large family of RTKs composed of alternatively spliced isoforms of four genes (*Fgfr1b-c*, *Fgfr2b-c*, *Fgfr3b-c*, *Fgfr4*), where the "b" and "c" isoforms are expressed mainly on epithelial and mesenchymal cells, respectively (Ornitz & Itoh, 2015). More than 22 FGF ligands exist (Ornitz & Itoh, 2015), making FGF/FGFR an ideal system to study trafficking-dependent signalling integration. FGFRs play an important yet understudied role in breast cancer and are deregulated in a significant percentage of the estrogen/progesterone receptor (ER/PR) and Triple Negative Breast Cancer (TNBC) subtypes of breast cancer (Babina & Turner, 2017; Navid *et al*, 2020). Furthermore, FGFs are essential for proficient breast cancer organoid growth (Sachs *et al*, 2018), but their role *in vivo* is less clear (Clayton & Grose, 2018; Navid *et al.*, 2020; Watson & Francavilla, 2018). Although breast cancer is known to have deregulated RTK signalling and trafficking (Butti *et al*, 2018), the functional consequences of recycling in breast cancer cells are yet to be determined. It is also unclear how ligand, receptor- and protein adaptors integrate trafficking and signalling to fine-tune breast cancer cellular responses. Therefore, to dissect recycling-dependent integration of signalling outputs from multiple angles we developed three quantitative Trafficking Phosphoproteomics Approaches (TPAs), which focused on recycling FGFs-, recycling FGFRs-, and recycling adaptor-dependent signalling (Figure 1A). To our knowledge, previous global studies of the trafficking-signalling enigma focused on a single question, either uncovering general trafficking regulators by genetic screening or multiparametric imaging analysis (Collinet *et al*, 2010; Gut *et al*, 2018; Liberali *et al*, 2014) or revealing the partners of trafficking effectors by proximity labelling methods (Gillingham et al, 2019). Here, we constructed for the first time a snapshot of FGFR recycling-dependent signalling in breast cancer cells and provided a comprehensive resource for the trafficking, signalling, and cancer communities. We unexpectedly identified a novel signalling interplay between FGFR and EGFR from the recycling endosomes. Specifically, FGFR recycling ligands induce phosphorylation on EGFR at the non-catalytic threonine T693 (T669 in the Uniprot sequence P00533) that reciprocally affects both FGFR and EGFR signalling outputs in breast cancer cells. We have therefore elucidated reciprocal priming between FGFR and EGFR which is based on an early phosphorylation-dependent signal and which coordinates trafficking-dependent signalling outputs.

RESULTS

TPAs Unmask FGFR-dependent EGFR_T693 Phosphorylation

To investigate recycling-dependent signalling in breast cancer cells we compared the FGFR2b recycling stimulus FGF10 to FGF7, which induces FGFR2b degradation (Francavilla *et al.*, 2013) (Figure 1B-C, Appendix Figures S1A-B), and analysed changes in the global signalling of a panel of five FGFR2b-expressing breast cancer cell lines (Francavilla *et al.*, 2013) (Appendix Figure S1C). The breast cancer cell lines were treated with FGF7 or FGF10 for 1 or 8 min. and such early signalling was analysed using phosphoproteomics, hereafter referred to as Trafficking Phosphoproteomics Approach 1 (TPA1) (Figure 1A). TPA1 showed a high degree of reproducibility in four independent experiments with the identification of phosphorylated peptides in the high intensity range and the quantification of 4559 proteins and 9494 phosphorylated sites in total, consistent with previous publications (Lundby *et al.*, 2019) (Appendix Figure S1C-I, Datasets EV1-2). Hierarchical clustering of the differentially regulated

phosphorylated sites showed clustering of breast cancer cell lines based on their known molecular subtypes (Neve *et al*, 2006), within which we identified clusters based on FGFR2b-specific early signalling (Appendix Figure S2A). We focused on the 5 cell-line specific FGFR2b signalling clusters identified across the breast cancer cell lines (32.5% of the phosphoproteome) and found an enrichment for proteins involved in signalling pathways, adhesion, and establishment of localization (endocytosis and transport) common to all cell lines (Appendix Figure S2B). Within these 5 clusters 78 kinases were identified as being phosphorylated (Appendix Figure S2C) and 12 of them were associated to the Gene Ontology (GO) terms establishment of localization and/or adhesion - including EGFR - consistent with enrichment of all proteins (Appendix Figure S2B-C). To study the differential phosphoproteomes downstream from FGF7 and FGF10 we focused on T47D and BT20. Each cell line represents a distinct breast cancer molecular subtype (Neve *et al.*, 2006), mirrored in FGFR2b-specific clusters (Appendix Figure S2A). Furthermore, these cell lines express different levels of *Fgfr2b* (Appendix Figure S2D) and respond to FGF7/10 stimulation, as shown by increasing phosphorylation of ERK and cell proliferation (Watson & Francavilla, 2018) (Figure 1D, Appendix Figure S2E-G). Interestingly, hierarchical clustering showed that each FGF separated the phosphoproteome to a greater extent than the duration of stimulation (Figure 1E-F, Appendix Figure S2H-I), confirming the uniqueness of ligand responses (Francavilla *et al.*, 2013). Analysis of the FGF7- and FGF10-specific clusters showed enrichment of the GO term protein localization unique to FGF10 stimulation in both T47D and BT20 (Figure 1E-F, Appendix Figure S2H-I). In support of the idea that the FGF10 phosphoproteome regulates protein localization in breast cancer cells, we found that the FGF10 phosphorylated proteins were enriched in all cellular compartments including endosomes, and that 63% of them were ascribed to human diseases, including breast cancer (Pletscher-Frankild *et al*, 2015) (Figure 1G). Furthermore, the FGF10-regulated phosphoproteome in T47D and BT20 contained TTP and RCP (Figure 1G), known to regulate FGFR2b and EGFR recycling, respectively (Francavilla *et al.*, 2016; Francavilla *et al.*, 2013). Confocal microscopy confirmed that FGF10-induced FGFR2b recycling required TTP (Francavilla *et al.*, 2013), but also RCP (Figure 1H-I, Appendix Figure S2J). Altogether, these data highlight a role for TTP and RCP in FGFR2b trafficking and early signalling specifically induced by the recycling ligand FGF10 in breast cancer cells.

Next, we studied how widely recycling affects signalling in breast cancer cells by assessing the contribution of three recycling FGFRs and of the recycling adaptors TTP and RCP to changes in the phosphoproteome, hereafter referred to as TPA2 and TPA3, respectively (Figure 1A, Datasets EV3-5). TPA2 compares the signalling downstream of recycling FGFRs in a defined genetic background. We overexpressed FGFR1c, 2b, or 4 in BT549 cells, which lack these FGFRs, and stimulated cells with Enkamin-E, FGF10 or FGF1 for 8 and 40 min., respectively (Figure 2A). It is known that each of these ligands induced recycling of the paired receptor (Francavilla *et al.*, 2016; Francavilla *et al.*, 2013; Haugsten *et al*, 2005) and we showed also ligand-dependent sustained signalling activation (Appendix Figure S3A-B). Hierarchical clustering of the 6402 phosphorylated sites from this high-quality dataset (Appendix Figure S3C-H), identified a cluster related to early signalling (8 min.) and one associated with late endosomal signalling (40 min.) common to all the considered FGFR-ligand pairs (Figure 2B). Refined analysis of this Recycling Receptor Cluster revealed a signalling network of 866 proteins of

which 38 were known trafficking proteins and 24, among which EGFR, TTP, and RCP, were also identified by TPA1 (Figures 1, 2C, and Appendix Figures S1, S2, S3I). TPA3 analysed the FGF10-dependent phosphoproteome of T47D in the presence or absence of the recycling adaptors TTP or RCP (Figure 2D, Appendix Figure S3J). We identified 9569 phosphorylated sites and verified the high-level of correlation between replicates of TPA3 (Appendix Figure SI-O). Hierarchical clustering identified TTP and RCP specific clusters and a common Recycling Adaptors Cluster (Figure 2E). The analysis of 113 proteins associated to the GO term establishment of localization in the latter cluster revealed 22 proteins already identified by TPA1, of which 6 were kinases, including EGFR (Figures 1, 2F, and Appendix Figures S1, S2, S3P). To identify key regulators of signalling downstream from FGFR recycling in breast cancer cells based on the multi-angle TPAs we focused on phosphorylated proteins belonging to the GO term establishment of localization and prioritized the 22 phosphorylated proteins in common to the three TPAs (Figure 2G). This group of proteins included scaffolding proteins and the three protein kinases AKT, PAK1 and, strikingly, EGFR (Figure 2G). Assessment of EGFR phosphorylated sites that were differentially regulated within each TPA highlighted that the phosphorylation of the non-catalytic threonine 693 (EGFR_T693) was uniquely associated with a recycling signature (40 min. upon stimulation) (Figure 2G). Therefore, the three quantitative TPAs developed to study FGFR recycling-dependent signalling integration in breast cancer cells (Figure 1A) unveiled a FGFR recycling-associated EGFR_T693 phosphorylation (Figures 1G, 2C, 2F, 2G, and Datasets EV1-5). This finding suggests a hitherto unknown signalling interplay between FGFRs and EGFR in breast cancer cells. As EGFR_T693 phosphorylation is critical for EGF-induced EGFR internalization (Heisermann *et al*, 1990) and is induced by the EGFR recycling stimulus TGFα in a sustained manner (Francavilla *et al.*, 2016), we hypothesized that EGFR_T693 phosphorylation may contribute towards FGFR outputs that depend on FGFR recycling.

EGFR_T693 Phosphorylation is FGFR2b Ligand-, Recycling-, and Activation-Dependent

To verify the potential interplay between FGFR and EGFR we first validated EGFR_T693 phosphorylation in T47D, BT20, HA-FGFR2b-BT549, and a breast cancer organoid grown from a TNBC patient-derived xenograft (PDX) tumour (Eyre *et al*, 2016). FGF10, but not FGF7, induced EGFR phosphorylation on T693, whilst leaving the catalytic residue tyrosine 1068 (Y1068) unaltered at 40 min. stimulation (Maennling *et al*, 2019). By contrast, the EGFR ligands EGF and TGFα induced the phosphorylation of both T693 and Y1068, as shown previously (Ceresa & Peterson, 2014) (Figure 2H-I). Therefore, sole phosphorylation of EGFR at T693 is FGF10/FGFR2b-specific.

To confirm that FGF10-induced FGFR2b recycling was involved in EGFR_T693 phosphorylation we depleted TTP or RCP and stimulated T47D and BT20 with FGF10 for 40 min. This resulted in decreased EGFR_T693 phosphorylation and ERK activation upon depletion of either recycling adaptor (Appendix Figure S4A-B). Overexpressing siRNA resistant TTP or RCP restored both EGFR_T693 phosphorylation and ERK phosphorylation following FGF10 stimulation (Figure 2J). Furthermore, we observed a peak in EGFR_T693 phosphorylation at 40 min. post-stimulation with FGF10 - when FGFR2b was present in recycling endosomes (Figure 1B-C-H-I, Appendix Figure S4C). Finally, FGF10-

mediated phosphorylation of EGFR_T693 decreased when FGFR2b trafficking was inhibited by dominant negative Rab11 (preventing recycling) or dominant negative Dynamin (preventing internalization) with no discernible alterations in ERK activation (Appendix Figure S4D-G). As TGFα or EGF induced EGFR_T693 phosphorylation occurs regardless of length of stimulation, or trafficking inhibition (Figure 2J, Appendix Figure S4) we concluded that EGFR_T693 phosphorylation is independent of EGFR recycling, but FGFR2b-induced phosphorylation of EGFR on T693 requires recycling upon FGF10 stimulation.

We next verified whether the kinase activity of FGFR was required for EGFR_T693 phosphorylation. Enkamin-E, FGF10, and FGF1 induced EGFR_T693 phosphorylation in cells expressing their cognate receptors, but this was suppressed by the FGFR inhibitor PD173074 (Pardo *et al*, 2009) (Figure 3A-B). Similarly, FGF10-dependent EGFR_T693 phosphorylation decreased in cells transfected with the catalytically inactive HA-FGFR2b_Y656F/Y657F (Francavilla *et al.*, 2013) (Figure 3C). Furthermore, FGF10, but not TGFα, required FGFR activation to induce EGFR_T693 phosphorylation and ERK activation in breast cancer cells expressing endogenous FGFR2b (Figure 3D). Conversely, TGFα-, but not FGF10-induced EGFR_T693 phosphorylation was blocked by the EGFR inhibitor AG1478 (Han et al, 1996) (Figure 3D). These data suggest that EGFR_T693 phosphorylation downstream from FGFR ligands depends on FGFR but not EGFR activation. As a conserved proline follows T693 on EGFR and TPA2-3 uncovered an ERK-kinase-substrate (or proline in +1) motif encompassing the phosphorylated EGFR (Figure 2C-F, 3E), we treated T47D and BT20 with MEK inhibitors, U0126 and MEK162 (Cheng & Tian, 2017), or the p38 kinase inhibitor BMS582949 (Emami *et al*, 2015) (Figure 3A). Both MEK inhibitors blocked ERK phosphorylation in cells stimulated with FGF10 and TGFα, and EGFR_T693 phosphorylation was simultaneously decreased upon FGF10 treatment, and to lesser extent upon TGFα, whereas p38 inhibition had no effect (Figure 3F-G). Therefore, EGFR_T693 phosphorylation depended on MEK-ERK, but not p38, signalling upon FGF10 stimulation.

In conclusion, FGF ligands which induce the recycling of their paired FGFR receptor increase EGFR_T693 phosphorylation via FGFR and ERK signalling, independent of EGFR or p38 activity.

FGF10 Primes EGFR Responses

To explore the consequences of the FGFR and EGFR interplay we first tested the effect of FGF10 on EGFR functions. FGF10 stimulation did not alter the levels of EGFR, which decrease over time upon EGF - and to a lesser extent TGFα - stimulation (Francavilla *et al.*, 2016) (Figure 4A). However, if T47D cells were pre-treated for 40 min. with FGF10, followed by stimulation with EGF for different time points, we observed an increase in EGFR abundance and ERK activation relative to cells not pre-treated with FGF10 for 120 min. (Figure 4B). FGF10 pre-treatment did not have the same effect on EGFR stabilization from the recycling stimulus TGFα at 120 min and a less pronounced effect on ERK phosphorylation at any time point. These data suggest that FGF10 pre-treatment alters EGF signalling to increase stability of EGFR at 120 min resulting in higher levels of ERK activation. FGFR2 levels remained high with all treatment conditions, however 40 min. FGF10 pre-treatment did alter the dynamics of FGFR2b downstream of both EGF and TGFα stimulation. The effect of FGF10 pre-

treatment on EGFR dynamics in EGF-stimulated cells depended on both FGFR and ERK activities (Figure 4C-D). When EGFR was stabilized with AG1468 (Gan et al., 2007), the stability of the EGFR following pre-treatment was in line with FGF10 40 min. stimulation, whereas ERK activation decreased (Figure 4E). Therefore, FGF10 pre-treatment increases the total levels of EGFR after EGF-stimulation, and this resulted in sustained ERK phosphorylation, an effect dependent on the activation of the FGFR-ERK signalling axis. Correspondingly, FGF10 pre-treatment followed by EGF stimulation for 4h induced the highest expression of ERK late target genes (Uhlitz et al, 2017) (Figure 4F), which may suggest enhanced cell cycle progression (Sharrocks, 2006). This was confirmed by increased EdU incorporation in T47D and BT20 stimulated with EGF upon pre-treatment with FGF10 (Figure 4G, Appendix Figure S5A). The use of specific inhibitors indicated that FGF10 significantly increased EGF-dependent cell cycle progression in an FGFR-, ERK-, and EGFR-dependent manner (Figure 4G-H and Appendix Figure S5).

In conclusion, FGF10 pre-treatment stabilizes EGF-stimulated EGFR via FGFR-ERK signalling. Elevated ERK phosphorylation, increased expression of ERK late target genes, and enhanced cell cycle progression suggest that FGF10 pre-treatment primes EGF responses and confirms a functional interplay between FGFR and EGFR signalling.

FGF10-dependent EGFR_T693 Phosphorylation in the Recycling Endosomes Reciprocates Priming of FGFR2b Outputs

The FGFR/EGFR interplay was also verified by uncovering the co-localization of FGFR2b with EGFR in recycling endosomes upon 40 min. stimulation with FGF10, but not with TGFα (Figure 5A-B, Appendix Figure S6A-B). Intriguingly, EGFR was phosphorylated on T693 in recycling endosomes at 40, but not at 20 min., in response to FGF10 (Figure 5C-D, Appendix Figure S6C). We therefore hypothesized that the recycling endosomes may form the interface for FGFR and EGFR signal integration, perhaps involving physical interaction of the receptors, and that EGFR_T693 phosphorylation could affect FGFR2b trafficking. We assessed FGFR2b/EGFR co-localization and co-immunoprecipitation in T47D cells depleted of endogenous EGFR and transfected with either EGFR wild type (wt) or the T693A mutant (T693A) - which cannot be phosphorylated at residue T693 - upon a time-course stimulation with FGF10 (Figure 5, Appendix Figure S6, Appendix Figure S7A-B). Under non-stimulated conditions FGFR2b co-localized at the plasma membrane and co-immunoprecipitated with both wt and T693A EGFR (Figure 5E-G, Appendix Figure S6D-F). At 20 min. stimulation with FGF10, FGFR2b was detected in the recycling endosomes in both wt- and T693A-expressing cells, but it failed to interact or localize with either EGFR as both were still located at the plasma membrane (Figure 5E-F, Figures EV1-2, Appendix Figure S6G). Therefore, FGFR2b traffics to the recycling endosomes before interacting with EGFR. We also observed that FGFR2b localization to the recycling endosomes in FGF10 stimulated wt-expressing cells for 40 min. was lost in the presence of T693A. At this time point FGFR2b co-immunoprecipitated with both wt and T693A (Figure 5G), but co-localized with wt in recycling endosomes and with T693A at the plasma membrane. These data imply that FGFR2b trafficking is altered in cells expressing T693A EGFR. Interestingly, RCP failed to interact with FGFR2b in T693A-expressing cells stimulated for 40 min. with FGF10 (Figure 5G, Appendix Figure

S6F, suggesting that RCP and EGFR interact with FGFR2b in recycling endosomes in a T693 phosphorylation-dependent manner. Finally, at 60 min stimulation with FGF10, we detected FGFR2b and EGFR at the plasma membrane in both wt- and T693A-expressing cells (Figure 5E-G, Appendix Figure S6F-G). TGFα stimulation of T693A-expressing cells confirmed that T693 phosphorylation regulates EGFR internalization (Heisermann *et al.*, 1990), as the T693A receptor was unable to traffic from the plasma membrane under any of the tested conditions (Figure 5E-F). Using GFP-Rab11-APEX2, which did not affect FGFR2b trafficking (Appendix Figure S6H), we assessed at which time point the majority of EGFR phosphorylated on T693 was detected in proximity to the recycling endosomes following FGF10 stimulation. In agreement with the confocal imaging, we found that EGFR phosphorylation on T693 accumulated at the recycling endosomes between 20 and 40 min. stimulation, when FGFR2b was detected in recycling endosomes together with RCP (Appendix Figure S6G-I, Figure 5). Altogether, these data suggest that EGFR_T693 phosphorylation dynamically regulates FGFR2b trafficking after the formation of an FGFR2b/EGFR/RCP complex in the recycling endosomes. Indeed, in T693A-expressing and in cells treated with FGFR and ERK inhibitors, but not EGFR or p38 inhibitors, there is less intracellular FGFR2b and increased receptor at the cell surface at 40 min. stimulation (Figure 5H, Appendix Figure S6J-K). Therefore, FGF10-dependent EGFR_T693 phosphorylation via FGFR and ERK activation (Figure 3) plays a role in the spatio-temporal regulation of FGFR2b trafficking.

To test the cellular impact of FGFR/EGFR signalling integration by quantifying whether EGFR_T693 phosphorylation affects FGF10 signalling downstream from FGFR2b, we compared the phosphoproteome of T47D expressing either wt or T693A EGFR upon stimulation with FGF10 for 40 or 60 min. (Figure 6A, Dataset EV6). We confirmed the absence of T693 phosphorylation of T693A EGFR, whilst other EGFR residues and ERK were phosphorylated in both wt- and T693A-expressing cells (Appendix Figure S7A-B). The reproducibility of this dataset was consistent with the previous ones (Appendix Figures S1-3, S7C-G, Datasets EV1-6). Hierarchical clustering of the 6485 identified phosphorylated sites revealed 4 clusters. Three clusters grouped sites whose phosphorylation increased in T693A- compared to wt-expressing cells. These clusters (Plasma Membrane Response, Acquired Response, and Late Response) were enriched for general cellular processes (Figure 6B-C). The fourth cluster (T693 Phosphorylation-Dependent Response) represented phosphorylation sites dependent on EGFR_T693 phosphorylation downstream from FGF10 signalling (Figure 6B-C). Of the 102 phosphorylated sites identified on the 53 kinases within all the four clusters, 10 were known regulatory sites (Figure 6D, Datasets EV6-7). More specifically, FGF10-stimulated T693A-expressing cells showed decrease phosphorylation of proteins belonging to the GO term cell cycle, including the activating T161 site on the cell cycle regulator cyclin-dependent kinase 1 (CDK1) (Coulonval *et al*, 2011) (Figure 6D, S7H, Dataset EV7). We confirmed that FGF10 induced CDK1_T161 phosphorylation in wt-, but not T693A-expressing T47D and BT20 cells (Figure 6E-F). Furthermore, FGF10-mediated cell cycle progression decreased in T693A-expressing cells, an effect due to impaired EGFR_T693 phosphorylation, as the total level of EGFR wt or T693A did alter over time (Figure 7A-B, S7I). Therefore, FGF10-mediated FGFR2b recycling, CDK1 phosphorylation, and the level of cell cycle progression all depend on EGFR_T693 phosphorylation. Finally, FGF10-dependent EGFR_T693 phosphorylation plays a crucial role in FGF10 priming of EGFR responses, as shown by decreased

EdU incorporation in T693A-expressing T47D and BT20 cells stimulated with FGF10 for 40 min prior to TGFα treatment (Figure 7C-D). We have previously shown that FGF10-mediated FGFR2b recycling regulates cell migration (Francavilla *et al.*, 2013) and RTK recycling is known to increase cell motility (Crupi et al, 2020). As FGFR2b recycling was impaired in T693A-expressing cells (Figure 5), we then investigated whether EGFR_T693 phosphorylation was required for cell invasion. Surprisingly, FGF10 stimulation increased cell invasion in both wt- and T693A-expressing cells (Figure 7E-F), implying that EGFR_T693 phosphorylation is not important for FGF10-induced cell invasion. In conclusion, our data showed that recycling endosomes facilitate EGFR_T693 phosphorylation induced by FGF10 and that T693 phosphorylation is required for the full response to FGF10 and for FGF10 to prime EGF responses (Figure 7G, Figure EV3).

Overall, the "reciprocal priming" between FGFR and EGFR is a novel mechanism to coordinate the trafficking and the signalling outputs of these two RTKs in breast cancer cells.

Discussion

This study shows that FGFR activation primes EGF-mediated responses in breast cancer cells whilst inducing EGFR_T693 phosphorylation from the recycling endosomes. Such phosphorylation events in turn modifies the FGFR responses. This reciprocal priming between FGFR and EGFR from the recycling endosomes alters the dynamics of recycling and enhances cell cycle progression, but not cell invasion, downstream from both RTKs. It represents the first early, selective and multi-functional mechanism of RTK signalling integration which drives long-term outputs. In contrast to the known RTK cross-talk, where the inhibition of a dominant RTK may result in the compensatory recruitment of signalling molecules to a second RTK (Cao, 2016), reciprocal priming does not occur sequentially, rather simultaneously during the entry route of each RTK into the cytoplasm. This is an efficient way to rapidly change cell behaviour in response to the presence of a combination of ligands in the cell environment. Based on our comprehensive resource which integrates four quantitative phosphoproteomics datasets we suggest that several recycling and signalling factors identified in this study may play a role in ensuring the co-localization of RTKs in the same cellular compartment. TPAs can be also explored by the community to pinpoint the molecular determinants of RTK recycling-dependent signalling in breast cancer cells. We therefore envision that reciprocal priming discovered in this study is unlikely to be restricted to FGFR and EGFR, opening up an exciting and novel avenue of RTK biology to be investigated. For instance, it remains to be determined whether FGFs induce the phosphorylation of threonine residues via ERK activity also on other RTKs. The discovery of a similarly phosphorylated peptide on c-Met depending on FGFRs recycling (Figure 2C, Dataset EV4) and on other members of the EGFR family (Figure 3E) suggests the presence of a network among RTKs in the recycling endosomes.

Besides regulating EGFR trafficking (Heisermann *et al.*, 1990), T693 phosphorylation is a highly conserved residue (see Review Process File) and involved in the response to stress or to the anti-tumour agent cisplatin via p38 activation (Winograd-Katz & Levitzki, 2006; Zwang & Yarden, 2006). Here, we show that FGFR ligands can induce EGFR_T693 phosphorylation and that T693

phosphorylation is required for the full activation of FGF10 responses and for FGF10 priming of EGFR outputs. This increases the repertoire of stimuli, including tumour necrosis factor-α (TNFα) (Singhirunnusorn *et al*, 2007) or the Eph family (Stallaert *et al*, 2018), and the mechanisms which modulate EGFR activity with strong implications for RTK signalling integration. This concept is also supported by data showing that EGF-mediated phosphorylation of FGFR1 can be a route of RTK cooperation (Zakrzewska et al, 2013). Hence, further comprehensive studies are needed to fully understand how RTKs act in concert *in vivo* in response to the simultaneous presence of multiple ligands and how they ultimately regulate cell fate.

The dynamics of RTK trafficking is affected by several factors and in turns affects downstream signalling. For instance, EGFR recycles through recycling endosomes even in the absence of stimuli (Baumdick *et al*, 2015) and can be found in a subset of perinuclear compartments (Tomas *et al*, 2015). This potentially explains why the majority of EGFR_T693 phosphorylation is found at recycling endosomes upon FGF10 stimulation between 20 and 40 min., a time point when FGFR2b itself starts accumulating in the recycling endosomes. In turn, FGFR2b trafficking is deregulated when EGFR remains at the plasma membrane, e.g. in the absence of T693 phosphorylation, suggesting that the transient formation of the EGFR/FGFR2b complex on recycling endosomes is the key regulatory event for the correct *timing* of FGR2b trafficking. One alternative model is that FGFR2b is internalized, traffics back to the plasma membrane where it retrieves EGFR, then reinternalizes (potentially recycling together EGFR), but the reinternalization step stalls without phosphorylation at T693. Another possibility is that FGFR2b phosphorylates the EGFR to prevent its recycling to the plasma membrane, thus explaining the change in EGFR distribution. This process should be replicated in FGF7-stimulated cells and would require further validation by high-resolution imaging of pools of FGFR2b and EGFR from the plasma membrane to recycling endosomes and back. The phosphorylation of EGFR might delay FGFR recycling back to the plasma membrane, thus allowing the formation of specific signalling complexes at the recycling endosomes. The kinases AKT and PAK1 identified by the three TPAs experiments would be interesting candidates to focus on to test this hypothesis. The alteration of the kinase landscape shown in T693A-expressing cells (Figure 6D) also confirms the idea that the EGFR phosphorylation may work as a scaffold for the recruitment of recycling machinery (e.g. RCP) and signalling partners to FGFR2b. The hypothesis of a multi-step regulation of FGFR2b - and possibly other RTKs - recycling is supported by our data on TTP and RCP. FGFR2b was not detected in recycling endosomes in TTP-depleted cells (Figure 1H), therefore we propose that TTP is required for FGFR2b *entry* into recycling endosomes in epithelial cells (Figure 1I) (Francavilla *et al.*, 2013). This would explain the lack of T693 phosphorylation and FGFR2b degradation in the absence of TTP. The third player in the complex regulation of FGFR2b recycling is RCP, which is bound to FGFR2b and EGFR in the recycling endosomes. As FGFR2b localized to recycling endosomes in RCP-depleted cells (Figure 1H), but it is partially degraded in this condition (Figure 1I), RCP may play a role in FGFR2b *exit* from recycling endosomes. Therefore, RCP plays a temporally unique role in FGFR2b trafficking besides being a regulator of EGFR and integrin recycling (Caswell & Norman, 2008; Francavilla *et al.*, 2016). We speculate on the presence of different populations of endosomes, either leading to recycling to plasma membrane (RCP-positive) or to receptor degradation (RCP-negative), implying that different families of

RTKs regulate each other trafficking and signalling through a pool of adaptors on recycling endosomes. Future studies will reveal these adaptors upon different perturbations to build a more comprehensive regulatory network of RTK trafficking.

RTK recycling is known to control cellular responses, including proliferation, migration and invasion (Caswell & Norman, 2008; Francavilla *et al.*, 2016; Francavilla *et al.*, 2013). Here, we show that the multi-layered regulation of FGFR2b by ligand nature, trafficking route, and EGFR priming fine tune downstream responses. Whereas cell migration and invasion require a signal from FGFR2b in recycling endosomes (Francavilla *et al.*, 2013), the signal to fully promote the cell cycle occurs in a precise time window, when FGF10 primes FGFR2b and EGFR to recycling endosomes. As in the absence of the FGFR/EGFR reciprocal priming growth factors are less mitogenic but remain pro-migratory, we propose that recycling endosomes are dynamic signalling hubs that enable cells to coordinate cell cycle progression and cell invasion in response to multiple growth factors. Therefore, modulating RTK communication at early time windows might be an efficient way to re-direct cellular responses *in vivo*.

The simultaneous presence of RTKs has been described in breast cancer (Butti *et al.*, 2018), where it might account for response to combined therapies (Issa *et al*, 2013), acquired resistance (Hanker *et al*, 2017), and epithelial cell-stroma communication (Wu *et al*, 2018). However, the concept of reciprocal priming has not been explored yet. It might have implications in TNBC, where both FGFRs and EGFR are highly expressed (Butti *et al.*, 2018). Although we have not tested the effect of T693 phosphorylation in normal breast cells or in the stroma (Weber *et al*, 2005), this phosphorylated site may become a prognostic or predictive marker, if a correlation between T693 phosphorylation, clinical parameters, and the response to combined EGFR/FGFR therapies is determined. This idea is supported by the detection of T693 phosphorylation in 50% of the TNBC patient-derived samples analysed in two independent phosphoproteomics datasets (Huang *et al*, 2017; Mertins *et al*, 2016). Importantly, reciprocal priming of RTKs may have implications when only one receptor is targeted as part of personalized therapies, where knock on effects to other pathways are not explored until resistance mechanisms have arisen (Tan *et al.*, 2017). Targeting pan RTK trafficking (Porebska *et al*, 2018) and trafficking players, like TTP, RCP, and those identified by TPAs might open up novel therapeutic scenarios for treatment. Indeed, most of the recycling players identified here are mutated in breast cancer according to the COSMIC database (Tate *et al*, 2019) and the importance of trafficking proteins in breast cancer is emerging (Wittkowski *et al*, 2018).

Understanding the extent of RTK regulation “in the right place at the right time” (Barrow-McGee & Kermorgant, 2014) is key for the integration of early signalling and long-term responses in cancer cells. Here, we unveiled a new form of RTK communication, a reciprocal priming co-ordinated from the recycling endosomes. Thus, the integration of TPAs offers a wealth of new candidates to investigate the functional consequences of trafficking-mediated signalling and has the potential to guide individualized treatment in cancer and other disease (Butti *et al.*, 2018; Kobayashi *et al*, 2019).

MATERIAL AND METHODS

MATERIALS AVAILABILITY

Further information and requests for resources and reagents should be directed to and will be fulfilled by Chiara Francavilla by email at chiara.francavilla@manchester.ac.uk

REAGENTS AND TOOLS

This information is provided in a separate **Reagents and Tools Table**.

EXPERIMENTAL MODELS

Cell Culture and SILAC labelling

Human breast cancer cell lines were purchased from ATCC, authenticated through short tandem repeat (STA) analysis of 21 markers by Eurofins Genomics, checked monthly for mycoplasma via a PCR-based detection assay (Venor®GeM – Cambio), and grown in the indicated media supplemented with 2 mM L-glutamine and 100 U/ml penicillin, 100 µg/ml streptomycin and 10% fetal bovine serum. MCF-7 was grown in DMEM/F12. MDA-MB-415 and BT20 were grown in DMEM. HCC1937, T47D and BT549 were grown in RPMI. 1 mM sodium pyruvate was added to T47D.
For quantitative mass spectrometry, BT549 or T47D cells were labelled in SILAC RPMI (PAA Laboratories GmbH, Germany) supplemented with 10% dialyzed fetal bovine serum (Sigma), 2 mM glutamine (Gibco), 100 U/ml penicillin and 100 µg/ml streptomycin for 15 days to ensure complete incorporation of amino acids, which was verified by MS analysis. Three cell populations were obtained: one labelled with natural variants of the amino acids (light label; Lys0, Arg0), the second one with medium variants of amino acids (medium label; L-[13C6] Arg (+6) and L-[2H4]Lys (+4); Lys4/Arg6) and the third one with heavy variants of the amino acids (heavy label; L-[13C6,15N4]Arg (+10) and L-[13C6,15N2]Lys (+8); Lys8/Arg10). The light amino acids were from Sigma, while their medium and heavy variants were from Cambridge Isotope Labs (Massachusetts, US).

Breast cancer organoid culture and protein isolation

Organoids were generated from a triple negative breast cancer PDX tumour, BB6RC37 (Eyre *et al.*, 2016). The tumours were minced and digested using a tumour dissociation kit (Miltenyi Biotec) on an orbital shaker at 37ºC for 1-2 hours. The cells were sequentially strained through 100µm and 40µm meshes. 50,000 cells were resuspended in 50µl cold growth factor-reduced Matrigel (Corning 354230), set as domes in a 24-well plate for 30 minutes and cultured at 37°C in media as defined by (Sachs *et al.*, 2018). The organoids were cultured in media with or without FGF7/10 for 14 days and EGF/Heregulin were removed from the media 24 hours before lysates were obtained. Lysates were prepared by mechanically disaggregating the domes and digesting the Matrigel for 1 hour using dispase at 37°C (Stem Cell Technologies, 7913). Cells were washed in PBS and resuspended in lysis buffer as previously described (Santiago-Gomez *et al*, 2019).

QUANTITATIVE PHOSPHOPROTEOMICS

Experimental Design and Sample Preparation

TPA1: for each cell line and each stimulus we analysed duplicates for each time point, considering both 1 and 8 min. time points as representative of early signalling. Therefore, we compared four label-free samples for each stimulus in each cell line (Datasets EV1-2). The cell pellet was dissolved in denaturation buffer (6 M urea, 2 M thiourea in 10 mM HEPES pH 8). We obtained 1 mg of proteins from each sample. Cysteines were reduced with 1 mM dithiothreitol (DTT) and alkylated with 5.5 mM chloroacetamide (CAA). Proteins were digested with endoproteinase Lys-C (Wako, Osaka, Japan) and sequencing grade modified trypsin (modified sequencing grade, Sigma) followed by quenching with 1% trifluoroacetic acid (TFA). Peptides were purified using reversed-phase Sep-Pak C18 cartridges (Waters, Milford, MA) and eluted with 50% acetonitrile (ACN). After removing ACN by vacuum concentrator at 60°C, peptides were suspended in phosphopeptides immunoprecipitation buffer (50 mM MOPS pH 7.2, 10 mM sodium phosphate, 50 mM NaCl) and dissolved overnight. Clarified peptides were transferred in a new tube containing immobilized phosphorylated tyrosine antibody beads (pY100-AC, Cell Signalling Technologies) and incubated for two hours at 4°C. After five washes with immunoprecipitation buffer followed by two washes with 50 mM NaCl, the enriched peptides were eluted from the beads three times with 50 µL of 0.1% TFA, loaded on C18 STAGE-tips, and eluted from STAGE-tips with 20 µL of 40% ACN followed by 10 µL 60% ACN and reduced to 5 µL by SpeedVac and 5 µL 0.1% formic acid (FA) 5% ACN added. Peptides from the supernatant were purified using reversed-phase Sep-Pak C18 cartridges (Waters, Milford, MA) and eluted with 50% ACN and further enriched for phosphorylated serine- and phosphorylated threonine-containing peptides, with Titansphere chromatography. Six mL of 12% TFA in ACN was added to the eluted peptides and subsequently enriched with TiO2 beads (5 µm, GL Sciences Inc., Tokyo, Japan). The beads were suspended in 20 mg/mL 2,5-dihydroxybenzoic acid (DHB), 80% ACN, and 6% TFA and the samples were incubated in a sample to bead ratio of 1:2 (w/w) in batch mode for 15 min with rotation. After 5 min centrifugation the supernatant were collected and incubated a second time with a two-fold dilution of the previous bead suspension. The beads were washed with 10% ACN, 6% TFA followed by 40% ACN, 6% TFA and collected on C8 STAGE-tips and finally washed by 80% ACN, 6% TFA. Elution of phosphorylated peptides was done with 20ul 5% NH3 followed by 20 µL 10% NH3 in 25% ACN, which were evaporated to a final volume of 5 µL in a sped vacuum. The concentrated phosphorylated peptides were acidified with addition of 20 µL 0.1% TFA, 5% ACN and loaded on C18 STAGE-tips. Peptides were eluted from STAGE-tips with 20 µL of 40% ACN followed by 10 µL 60% ACN and ACN and reduced to 5 µL by SpeedVac and 5 µL 0.1% FA, 5% ACN added.

A small amount of the eluted peptides (1%) was taken for proteome analysis before enrichment of phosphorylated peptides: after evaporation in a speed vacuum, 40 µL of 0.1% TFA, 5% ACN were added followed by MS analysis.

TPA2: we analysed label-free triplicates for each condition, T47D depleted or not of TTP or RCP and stimulated or not with FGF10. Cells were washed with PBS and lysed at 4°C in ice-cold 1% triton lysis buffer supplemented with Pierce protease inhibitor tablet (Life Technologies) and phosphatase inhibitors: 5 nM Na3VO4, 5 mM NaF and 5 mM β-glycerophosphate. Proteins were precipitated overnight at -20°C in four-fold excess of ice-cold acetone. The acetone-precipitated proteins were

solubilized in denaturation buffer (10 mM HEPES, pH 8.0,6 M urea, 2 M thiourea) and 5 mg of proteins were reduced, alkylated, and digested, as described above. All the steps were performed at room temperature. The peptide mixture was desalted and concentrated on a C18-SepPak cartridge, eluted, and enriched with TiO2 beads, as described above.

TPA3: we analysed duplicates of SILAC-labelled BT549, transfected and treated as described in Figure 2A. We followed the same procedure described for TPA2 with the only difference that 5 mg of each SILAC-labelled lysates were mixed in equal amount before digestion and TiO2 chromatography.

EGFR- and EGFR T693A-expressing T47D cells: we analysed duplicates of SILAC-labelled T47D transfected and treated as described in Figure 6A. We followed the same procedure described for TPA1 with the only difference that 5 mg of each SILAC-labelled lysates were mixed in equal amounts before digestion and phosphorylated tyrosine enrichment followed by TiO2 chromatography and peptides purification.

Mass Spectrometry

Purified peptides were analysed by LC-MS/MS using an UltiMate® 3000 Rapid Separation LC (RSLC, Dionex Corporation, Sunnyvale, CA) coupled to a QE-HF (Thermo Fisher Scientific, Waltham, MA) mass spectrometer. Mobile phase A was 0.1% FA in water and mobile phase B was 0.1% FA in ACN and the column was a 75 mm x 250 µm inner diameter 1.7 µM CSH C18, analytical column (Waters). A 1µl aliquot of the sample (for proteome analysis) or a 3µl aliquot was transferred to a 5µl loop and loaded on to the column at a flow of 300nl/min at 5% B for 5 and 13 min, respectively. The loop was then taken out of line and the flow was reduced from 300nl/min to 200nl/min in 1 min., and to 7% B. Peptides were separated using a gradient that went from 7% to 18% B in 64 min., then from 18% to 27% B in 8 min. and finally from 27% B to 60% B in 1 min.. The column was washed at 60% B for 3 min. and then re-equilibrated for a further 6.5 minutes. At 85 minutes the flow was increased to 300nl/min until the end of the run at 90min. Mass spectrometry data was acquired in a data directed manner for 90 min. in positive mode. Peptides were selected for fragmentation automatically by data dependent analysis on a basis of the top 8 (phosphoproteome analysis) or top 12 (proteome analysis) with m/z between 300 to 1750Th and a charge state of 2, 3 or 4 with a dynamic exclusion set at 15 sec. The MS Resolution was set at 120,000 with an AGC target of 3e6 and a maximum fill time set at 20ms. The MS2 Resolution was set to 60,000, with an AGC target of 2e5, and a maximum fill time of 110 ms for Top12 methods, and 30,000, with an AGC target of 2e5, and a maximum fill time of 45 ms for Top8 analysis. The isolation window was of 1.3Th (2.6 Th for SILAC-labelled samples) and the collision energy was of 28.

Raw Files Analysis

Raw data were analysed by the MaxQuant software suite (Cox & Mann, 2008) (https://www.maxquant.org; version 1.5.6.5) using the integrated Andromeda search engine (Cox et al, 2011). Proteins were identified by searching the HCD-MS/MS peak lists against a target/decoy version of the human Uniprot Knowledgebase database that consisted of the complete proteome sets and

isoforms (v.2016; https.//uniprot.org/proteomes/UP000005640_9606) supplemented with commonly observed contaminants such as porcine trypsin and bovine serum proteins. Tandem mass spectra were initially matched with a mass tolerance of 7 ppm on precursor masses and 0.02 Da or 20 ppm for fragment ions. Cysteine carbamidomethylation was searched as a fixed modification. Protein Nacetylation, N-pyro-glutamine, oxidized methionine, and phosphorylation of serine, threonine, and tyrosine were searched as variable modifications. Protein N-acetylation, oxidized methionine and deamidation of asparagine and glutamine were searched as variable modifications for the proteome experiments. For the quantification of SILAC-labelled samples labelled lysine and arginine were specified as fixed or variable modification, depending on prior knowledge about the parent ion (MaxQuant SILAC triplet identification). In all the other experiments, label-free parameters were used as described (Cox *et al*, 2014). False discovery rate was set to 0.01 for peptides, proteins and modification sites. Minimal peptide length was six amino acids. Site localization probabilities were calculated by MaxQuant using the PTM scoring algorithm (Olsen *et al*, 2006). The datasets were filtered by posterior error probability to achieve a false discovery rate below 1% for peptides, proteins and modification sites. Only peptides with Andromeda score >40 were included.

Data and Statistical Analysis

All statistical and bioinformatics analyses were done using the freely available software Perseus, version 1.6.5.0 or 1.6.2.1. (Tyanova & Cox, 2018), R framework (R Core Team, 2018), Bioconductor R-package LIMMA (Bolstad et al, 2003), WebGestalt (Liao et al, 2019), STRING (Szklarczyk *et al*, 2019), Cytoscape (version 3.7.2) (Shannon et al, 2003). All measured peptide intensities were normalized using the 'normalizeQuantiles' function from the Bioconductor Rpackage LIMMA, which normalizes the peptide intensities such that each quantile for each sample is set to the mean of that quantile across the dataset, resulting in peptide intensity distributions that are empirically identical. Each dataset was normalized individually. Subsequent data analysis was performed using Microsoft Office Excel, R and Perseus. For the SILAC datasets we used the normalized SILAC ratios from MaxQuant output txt files. Only peptides with localization probabilities higher than 0.75 (class I, shown in Datasets EV1, 3-6 ~~Supplementary Tables~~) (Olsen *et al.*, 2006) were included in the downstream bioinformatics analysis. Pearson correlation was calculated in R. For TPA1 we impute missing values using Perseus default settings, we subtracted the control from log intensity values in order to be able to compare all the cell lines against each other and we used the median for each condition. Hierarchical clustering based on correlation was performed after multi-sample ANOVA test with default parameters in Perseus. For TPA2 we calculated the median and then considered only rows with four valid values, followed by hierarchical clustering based on Euclidean distance in Perseus. For TPA3 and the EGFR/EGFR_T693A T47D dataset we imputed missing values using Perseus default settings and then calculated the median, followed by hierarchical clustering based on Euclidean distance in Perseus. Clusters used in the follow-up analysis were defined by Perseus and manually checked.

The enrichment of KEGG or GO terms was performed in WebGestalt using the ORA default parameters and significantly over-represented terms within the data were represented in bar plots. The relation of

genes to other diseases was based on the database DISEASES (Pletscher-Frankild *et al.*, 2015). All the protein interaction networks were obtained using the STRING protein interaction database using high confidence, and interactions derived from the Experiments and Databases evidence channels. Data visualization was performed using the software Cytoscape. The Venn diagram was created using the web tool http://bioinformatics.psb.ugent.be/cgi-bin/liste/Venn/calculate_venn.htpl.

BIOCHEMICAL AND FUNCTIONAL ASSAYS

RNA Isolation and real-time PCR analysis

RNA from cell lines was isolated with TRIZOL® (Invitrogen). After chloroform extraction and centrifugation, 5 µg RNA was DNase treated using RNase-Free DNase Set (Qiagen) and 1 µg of DNase treated RNA was then taken for cDNA synthesis using the Protoscript I first strand cDNA synthesis kit (New England Biolabs). Selected genes were amplified by quantitative real time PCR (RT-qPCR) using Sygreen (PCR Biosystems). Relative expression was calculated using the delta-delta CT methodology and beta-actin was used as reference housekeeping gene. Sequences for primers used can be found in the accompanying Reagent Table. qPCR machine used was Applied Biosystems MX300P.

Transfection and RNA interference.

All transfections were carried out in Gibco opti-MEM glutamax reduced serum media (ThermoFisher Scientific). For RNA interference, all cells were transfected using Lipofectamine RNAiMax (ThermoFisher Scientific), according to manufacturer instructions. Validated double-stranded stealth siRNA oligonucleotides were used for RNA interference. siRNA Universal Negative Control #2 (Sigma-Aldrich) was used as a control in all RNA interference experiments. BT549 and BT20 cells were transfected using Lipofectamine 3000 (ThermoFisher Scientific) according to the manufacturer's instructions, 24 h after RNA interference transfection where indicated. T47D cells were transfected using Escort IV according to manufacturer instructions, same as above. Assays were performed 36 h after transfection, as previously described (Francavilla *et al.*, 2016). Where assays were performed more than 36 h after transfection, RNAi and expression were assessed at time of assay to confirm expression.

Cell Lysis, Protein Immunoprecipitation, and Western Blotting

Cells were serum starved overnight in serum-free medium and stimulated for the indicated time points with 100 ng/mL of FGF7, FGF10, EGF or TGFα. Ligands were replenished every 24 h for long-term (24–72 h) stimulation. Where indicated, cells were pre-incubated for 2 h with 100 nM PD173074, 500 nM AG1478, 20 μM U1206, 1μM MEK162 or 10 μM BMS582949. Control cells were pre-incubated with DMSO alone. After stimulation, cell extraction and immunoblotting were performed as previously described (Francavilla *et al.*, 2016). Proteins were resolved by SDS-PAGE and transferred to nitrocellulose membranes (Protran, Biosciences). Proteins of interest were visualized using specific antibodies, followed by peroxidase- conjugated secondary antibodies and by an enhanced

chemiluminescence kit (Amersham Biosciences). Blots were visualized either using film exposure or the Universal Hood II Gel Molecular Imaging System (Bio-Rad). Each experiment was repeated at least three times and produced similar results.
Immunoprecipitation of FGFR2 from cell extracts was performed as previously described (Francavilla *et al.*, 2016), using anti BEK (Santa Cruz Biotechnology, sc-121). Each experiment was repeated at least three times and produced similar results.

Biotinylation assays

Biotinylation pull downs experiments were performed as described previously (Lobingier *et al*, 2017). Briefly biotinylation experiments were performed by transfecting GFP-Rab11-APEX2 constructs in to 2 million cells plated in 10cm dishes. Cells were pre-incubated (40 min.) with Biotin Phenol (Iris Biotech), after stimulation with ligands, Hydrogen peroxide (Sigma Aldrich) was added for 1 min. before quenching with Trolox (Sigma Aldrich) and Sodium ascorbate (VWR) during ice cold lysis. A 2 hour RT pull-down with streptavidin beads was then performed running the supernatant against the bound proteins.

Proliferation Assays

Incucyte cell-proliferation assay

Indicated cell lines were seeded into 24-well plates at a density of 15,000–20,000 cells per well, depending on growth rate and the design of the experiment. After plating cells were starved and stimulated with indicated ligands every 24 h and imaged every hour using the Incucyte ZOOM (Essen Bioscience) Phase-contrast images were analysed to detect cell proliferation based on cell confluence. And average confluency value over 4 h was used to determine the starting confluency from which a relative growth change was calculated. Statistical analysis was performed at the endpoint across repeats, as indicated in the figure legends.

Crystal Violet

Indicated cells were stained after experimentation by being fixed with 0.5 %w/v crystal violet (Sigma) in 4 %w/v paraformaldehyde/PBS for 30 minutes. Fixed cells were then solubilised in 2 %w/v SDS/PBS and absorbance measured at 595 nm using Synergy H1 microplate reader (BioTek). Statistical analysis was performed at the endpoint across repeats, as indicated in the figure legends.

EdU Incorporation

Indicated cells were labelled with 20 μM 5-ethynyl-2'-deoxyuridine (EdU) for 4 h and processed following the manufacturer's protocol (Click-iT® EdU Alexa Fluor® 488 Imaging Kit, Thermo Fisher). Prior to imaging cells were then stained with 5ng/ml Hoecsht 3342 for 15 minutes. Stained cells were analysed using a using a Leica microscope system. Statistical analysis was performed at the endpoint across repeats, as indicated in the figure legends.

Invasion Assay

Rat tail derived Collagen I (Corning) was supplemented with 25 µg/ml human fibronectin (Sigma) in DMEM and polymerised in 8µm transwell inserts (Corning) for 30 minutes at room temperature followed by 30 minutes at 37°C/5% CO2. 5 x 10^4 BT20 cells were seeded on the reverse of each insert and incubated for 6 hours at 37°C/5% CO2. Inserts were gently washed and placed in serum free DMEM and the upper chamber filled with DMEM supplemented with 10 % FCS (Life Technologies) and either PBS or 100ng/ml FGF10 (Peprotech). After 72 hours, cells were stained with 500ng/ml Calcein AM (Thermo Fisher) for 1 hour and visualised by Leica Sp8 inverted confocal microscopy in serial sections of 20 µm. Fluorescence intensity of each section was determined using Image J v. 1.52p (Schindelin *et al*, 2012) and proportion of invading cells estimated by comparing the total intensity beyond 40 µm with the total overall intensity per insert using GraphPad PRISM version 8.0.0.. Statistical analysis was performed at the endpoint across repeats, as indicated in the figure legends.

IMMUNOFLUORESCENCE

Immunofluorescence staining was performed as previously described (Francavilla *et al.*, 2016). To detect HA-FGFR2b or endogenous FGFR2 we incubated cells with 10 µg/ml of anti-HA (Covance) or anti-FGFR2 antibody (Cell Signalling) for 45 minutes with gentle agitation. The binding of the antibody did not activate receptor signalling in untreated cells nor induced receptor internalization (see control cells in Figure 1), as previously reported (Francavilla *et al*, 2009). After stimulation cells were incubated at 37°C for different time points. When indicated, each inhibitor was added prior stimulation. At each time point, non-permeabilized cells were either fixed to visualize the receptor on the cell surface (plasma membrane) or acid-washed in ice-cold buffer (50 mM glycine, pH 2.5) to remove surface-bound antibody. Acid-washed cells were then fixed and permeabilized to visualize the internalized receptor (cytoplasm). Finally, to detect FGFR2b cells were stained with AlexaFluor488-conjugated donkey anti-mouse or anti-rabbit (Jackson ImmunoResearch Laboratories). Nuclei were stained with DAPI. Coverslips were then mounted in mounting medium (Vectashield; Vector Laboratories).

For co-localization experiments, cells were acid washed, fixed, permeabilized with 0.02% saponin (Sigma), treated with a primary antibody against FGFR2, EGFR, TTP, RCP, phosphorylated T693 EGFR, EEA1 for 60 min at 37 °C, and stained with AlexaFluor488 (or 568 or 647)-conjugated donkey anti-mouse or anti-rabbit. Samples either expressing GFP-tagged proteins or treated with TRITC-transferrin or Alexa 647-transferrin (to stain transferrin receptor, Tf-R), added to the medium at a final concentration of 50 µg/mL, were kept in the dark. Nuclei were stained with DAPI. Coverslips were then mounted in mounting medium (Vectashield; Vector Laboratories).

All the images were acquired at room temperature on a Leica TCS SP8 AOBS inverted confocal using a 100x oil immersion objective and 2.5x confocal zoom. The confocal settings were as follows: pinhole, 1 airy unit, format, 1024 x 1024. Images were collected using the following detection mirror settings: FITC 494-530nm; Texas red 602-665nm; Cy5 640-690nm. The images were collected sequentially. Raw images were exported as .lsm files, and adjustments in image contrast and brightness were applied identical for all images in a given experiment using the freely available software Image J v.

1.52p (Schindelin *et al.*, 2012).

Quantification of the Recycling Assay

Quantification of recycling was performed as described (Francavilla *et al.*, 2016). For each time point and each treatment, the presence (total) and the localization (cell surface versus internalized) of HA-FGFR2 or endogenous FGFR2 were assessed in at least seven randomly chosen fields. Approximately 100 cells per condition (both acid washed and not) were analyzed from three independent experiments. The results are expressed as the percentage of receptor-positive cells (green) over total cells (corresponding to DAPI-stained nuclei) and referred to the values obtained at time zero. Statistical analysis was performed across repeats, as indicated in the figure legends.

Quantification of Expression Fraction, Overlap Fraction and Co-localization

Images were pre-processed using an "À trous" wavelet band pass filter to reduce the contribution of high frequency speckled noise to the co-localization calculations. Pixel intensities were then normalized from the original 8-bit range [0,255] to [0,1]. To ensure that co-localization was only computed in well-determined regions of interest (ROI), we used the Fiji/ImageJ (Schindelin *et al.*, 2012) built-in ROI manager to create and record these regions.

To measure differences in expression over time or between conditions, we computed the fractions of expressed red marker (R), green marker G. or far-red marker F. pixels over a region of interest (N_R, N_G or N_F pixels with a strictly positive intensity in N pixels):

$$F_R = \frac{N_R}{N} \quad F_G = \frac{N_G}{N} \quad F_F = \frac{N_F}{N}$$

To quantify the overlap fraction between two (R and G) or three (R, F and G) markers, we first multiplied the (normalized) channel intensities together, i.e. $I_{RG} = I_R \times I_G$ and $I_{RFG} = I_R \times I_F \times I_G$ to compute a new image whose intensity increases to 1 where the markers strongly overlap and decreases or becomes null for non-overlapping pixels. Our overlap fraction coefficient (OF) becomes the fraction of strictly positive pixels in the combined image over the number of pixels in the region of interest.

$$OF_{RG} = \frac{N_{RG}}{N} \quad OF_{RF} = \frac{N_{RF}}{N} \quad OF_{RFG} = \frac{N_{RFG}}{N}$$

Finally, Finally, to quantify the actual level of colocalization between two markers (e.g. R and G), we used the Manders Colocalization Coefficients (MCC) M1 and M2 (Manders et al, 1996). M1 measures the fraction of the R marker in compartments that also contain the G marker, and M2, the fraction of the G marker in compartments that also contain the R marker. Lower-bound thresholds for pixel intensities I_R and I_G were automatically determined using the Costes method (Costes et al, 2004).

Briefly,

$$M1 \cong \frac{\sum_{I_R > T_R} I_{R,C}}{\sum_{All\ I_R} I_R} \qquad M2 \cong \frac{\sum_{I_G > T_G} I_{G,C}}{\sum_{All\ I_G} I_G}$$

where with T_R and T_G are the threshold set by the automated Costes algorithm for the R and G channels, and $I_{R,C}$ and $I_{G,C}$ pixels are co-localized if their intensity in the reciprocal channel is above T_R or T_G set for that channel.

To measure the simultaneous overlap of our three, red, far-red and green markers (R, F, G), we first used the overlap image between marker R and marker F as defined above (i.e e. $I_{FR} = I_F \times I_R$). We then measured the MCC colocalization parameter of this combined image against a Green marker using the MCC formulae above, together with the Costes method to determine the T_{FR} and T_G thresholds.

The scripts for the quantification of co-localization were written in the Python language and the code for Costes-adjusted MCC was taken verbatim from the CellProfiler (McQuin *et al*, 2018) code base.

The Student's t-test was subsequently used to determine the difference in pixel overlap fraction or Manders (Costes) coefficient between different experimental conditions in Figures 1, 5, S4, S6.

DATA AVAILABILITY

The mass spectrometry proteomics data in Thermo Scientific's *.raw format have been deposited to the ProteomeXchange Consortium via the PRIDE (Perez-Riverol *et al*, 2019) partner repository with the dataset identifier PXD018184. Submission details: Project Name: Proximal Phosphoproteomics Approaches revealed a FGFR-EGFR functional cross-talk Project accession: PXD018184. ~~Reviewer account details. Username: reviewer32878@ebi.ac.uk. Password: Cifb7Nph.~~ To download: ftp://ftp.pride.ebi.ac.uk/pride/data/archive/2021/04/PXD018184

The scripts for the quantification of overlap fraction and co-localization are available on Github at the following address: https://github.com/manbio/smith_ferguson_coloc --

~~Original data will be submitted after publication:~~
~~https://data.mendeley.com/datasets/hvrzdgfnfy/draft?a=986c6543-36c6-4f22-929a-8a9dde81aa92~~

CONFLICT OF INTERESTS

The authors declare no conflict of interest.

ACKNOWLEDGEMENTS

We thank Profs. Lowe and Woodman, and Drs Caswell, Tournier and Lopez-Castejon for reading the manuscript and the Bioimaging and the Bio-MS Facilities (University of Manchester). Research in CF lab is supported by Wellcome Trust (WT Sir Henry Dale fellowship 107636/Z/15/Z), the Biotechnology

and Biological Sciences Research Council (BB/R015864/1), and Medical Research Council (MR/T016043/1). PhD students are supported by BBSRC Doctoral Training Programme (HF and JW: BB/M011208/1); Wellcome Trust (CB: 210002/Z/17/Z); CR-UK Non-Clinical Training Award (JP: A27445); and NIHR Manchester Biomedical Research Centre non-clinical PhD Studentship (TK: IS-BRC-1215-20007). RBC is supported by Cancer Research UK and Breast Cancer Now (MAN-Q2-Y4/5).

AUTHOR CONTRIBUTIONS

MPS performed experiments, supervised HRF, and helped writing the manuscript. HRF, JF, KK, TK, CB, JP, SC performed experiments. EZ quantified imaging data. JW helped with data analysis. PF contributed to sample preparation for MS analysis. SW and DK performed the MS experiments and provided technical advice. RC supervised TK. CF conceptualized the study, performed experiments, analysed the data, supervised PhD students, and wrote the manuscript. All the authors contributed to writing and approving the manuscript.

FIGURE LEGENDS

Figure 1. Trafficking Phosphoproteomics Reveals FGFR2b Recycling-dependent Outputs

A. Overview of the Trafficking Phosphoproteomics Approaches (TPAs).

B. Internalization (cytoplasm) and recycling (plasma membrane) of FGF7- and FGF10-stimulated endogenous FGFR2 (green) for 0, 15, 40, and 120 min. in T47D. TRITC-Tf is a marker of recycling (red). Nuclei are stained in blue. *, cells with receptor recycled to the plasma membrane. Scale bar, 5 μm.

C. Red and green pixels overlap fraction representing the co-localization of FGFR2b with the recycling endosomes marker Tf (above) and the proportion of green over total pixels representing FGFR2b in the cytoplasm (below) upon stimulation with FGF7 (dark green) or FGF10 (burgundy) for 15, 40, or 120 min.. Values represent the median ± SD of at least 3 independent experiments. Representative pictures are shown in B (cytoplasm). *, p value<0.005 (Student's t-test).

D. Confluence over time of BT20, T47D, and BT549 transfected with HA-FGFR2b stimulated with FGF7 (dark green) or FGF10 (burgundy). Data represent the mean ± SD of N=3 compared to FGF10. P value = <0.05 *, <0.01 **, <0.001*** (Student's t-test).

E. Hierarchical clustering of the phosphorylated sites differentially quantified T47D stimulated with FGF7 (green) or FGF10 (burgundy). Specific clusters are highlighted with black lines. The intensity of phosphorylated sites is presented on the logarithmic scale with intensity below and above the mean color-coded in blue and red, respectively.

F. Enriched terms in the selected clusters of E.

G. Network of phosphorylated proteins belonging to “protein localization” in FGF10 clusters, based on STRING, visualized in Cytoscape, and color-coded based on cell components. The squared shape represents phosphorylated proteins found in the database DISEASES. The recycling adaptors TTP and RCP are highlighted in grey.

H. Internalization (cytoplasm) and recycling (plasma membrane) of FGF10-stimulated HA-FGFR2b (green) transfected in BT549 stimulated for 0, 40 and 120 min.. Cells were depleted or not of TTP or RCP by a pool of siRNAs. TRITC-Tf is a marker of recycling (red). Nuclei are stained in blue. *, cells with receptor recycled to the plasma membrane. Scale bar, 5 μm.

I. The presence (total), internalization (internalized), and recycling (cell surface) of transfected HA-FGFR2b in BT549 upon stimulation were quantified as in (Francavilla *et al.*, 2016) and in the section “Quantification of the Recycling assay”. Values represent the median ± SD of N=3. Representative pictures upon FGF10 stimulation are shown in H.

Figure 2. TPA2-3 Unveil FGF10-dependent EGFR_T693 Phosphorylation

A. Experimental design of TPA2.

B. Hierarchical clustering of the phosphorylated sites differentially quantified in BT549 transfected with HA-FGFR1c, 2b, or 4 and stimulated for 8 or 40 min. with Enkamin-E, FGF10, or FGF1, respectively. Early Signalling and Recycling Receptors clusters are highlighted in light and medium blue, respectively. The intensity of phosphorylated sites is presented on the logarithmic scale with intensity below and above the mean color-coded in blue and red, respectively.

C. STRING-based and Cytoscape-visualized network of the phosphorylated proteins belonging to “endocytosis” (clusters medium blue in b). The diamond shape represents phosphorylated proteins found in TPA1. Kinases are highlighted in burgundy. The border is color-coded based on the substrate motifs.

D. Experimental design of TPA3.

E. Hierarchical clustering of the phosphorylated sites differentially quantified in T47D stimulated with FGF10 and depleted or not of TTP or RCP. The clusters for TTP Adaptors, RCP Adaptors or Recycling Adaptors are highlighted in orange, brown, and light green, respectively. The intensity of phosphorylated sites is presented on the logarithmic scale with intensity below and above the mean color-coded in blue and red, respectively.

F. STRING-based and Cytoscape-visualized network of phosphorylated proteins belonging to the Recycling Adaptors cluster (light green in E) and found in TPA1. Kinases are highlighted in burgundy. The border is color-coded based on the substrate motifs.

G. Venn diagram showing the phosphorylated proteins belonging to “establishment of localization” identified in TPA1-3 (left). STRING-based and Cytoscape-visualized network of the 22 proteins

identified by the 3 TPAs (centre). Phosphorylated sites quantified on EGFR (right). T693 is highlighted in yellow.

H-J. Lysates from (H) T47D, BT20, and HA-FGFR2b-transfected BT549 stimulated or not with FGF7, FGF10, EGF, and TGFα for 40 min.; (I) breast cancer organoid cultured from the PDX tumour BB6RC37 and grown for the last 24 hours as indicated; (J) control or 40 min. FGF10- or TGFα-stimulated T47D left untreated or depleted of TTP, followed or not by transfection with siRNA resistant Flag-TTP (Flag-TTP*) or depleted of RCP followed or not by transfection with siRNA resistant RCP-GFP (RCP-GFP*) were immunoblotted with the indicated antibodies. **, non-specific band (J).

Figure 3. FGF10-dependent EGFR_T693 Phosphorylation Requires FGFR and ERK

A. List of compounds and their targets.

B-D Lysates from BT549 transfected with HA-FGFR1c, 2b, or 4 and stimulated for 8 or 40 min. with Enkamin-E, FGF10, or FGF1, respectively, followed by treatment with either DMSO or the FGFR inhibitor PD173074 (B); BT549 transfected with HA-FGFR2b or HA-FGFR2b_Y656F/Y657F and stimulated with FGF10 for 40 min. (C); T47D treated with DMSO, PD173074 or the EGFR inhibitor AG1478 and stimulated or not with either FGF10 or TGFα for 0, 8, and 40 min. (D) were immunoblotted with the indicated antibodies.

E. Protein sequences surrounding T693 (based on Uniprot P00533) of members of the ErbB family were aligned using CLUSTAL O (version 1.2.4). The red box indicates that the amino acid T is followed by a conserved proline. Asterisks below the sequences indicate identical amino acid residues; double dots indicate conserved amino acid residues; single dots indicate semi-conserved substitutions.

F, G Lysates from T47D or BT20 treated with DMSO, PD173074, AG1478, or the MEK inhibitors U0126 and MEK162 and stimulated or not with either FGF10 or TGFα (F); T47D or BT20 treated with DMSO, or the p38 inhibitor BMS582949 and stimulated or not with either FGF10 or TGFα (G) were immunoblotted with the indicated antibodies.

Figure 4. FGF10 Primes EGFR Responses.

A-E Lysates from T47D stimulated or not with FGF10, EGF or TGFα for different time periods (A); pre-treated or not with FGF10 for 40 min. and either stimulated or not with FGF10, EGF or TGFα for different time periods (B) or treated with PD173074 (C), MEK162 (D), AG1478 (E) before stimulation were immunoblotted with the indicated antibodies.

F. Heatmap of the mRNA relative expression of the indicated ERK targets compared to control and quantified by qPCR. N=3. The minimum and maximum fold-induction is color-coded in white and burgundy, respectively.

G, H Percentage of EdU incorporation in T47D pre-treated or not with FGF10 for 40 min. and stimulated or not with FGF10 or EGF (G) or incubated with MEK162, PD173074, or AG1478 before pre-treatment (H). N= 6. P value = <0.05 *, <0.01 **, <0.001*** (one-way ANOVA with Tukey test).

Figure 5. EGFR_T693 Phosphorylation Regulates FGFR2b Recycling

A. Co-localization of FGFR2 (red), EGFR (green), and the recycling marker Tf (blue) in T47D stimulated or not with FGF10 or TGFα for 40 min. Scale bar, 5 μm.

B. Red and green pixels overlap fraction (above, left) representing the co-localization of FGFR2 with EGFR; red and far red pixels overlap fraction (above, right) representing the co-localization of FGFR2 with the recycling marker Tf; far red and green pixels overlap fraction (below, left) representing the co-localization of EGFR with the recycling marker Tf; green, red and far red pixels overlap fraction (below, right) representing the co-localization of FGFR2, EGFR, and the recycling marker Tf in T47D stimulated for 40 min. Values represent the median ± SD of at least 3 independent experiments. Representative pictures are shown in A and Appendix Figure S6A. *, p value<0.005 (Student's t-test).

C. Co-localization of EGFR (green), T693 phosphorylated EGFR (blue), and the recycling marker Tf (red) in T47D stimulated or not with FGF10 or TGFα for 40 min. Scale bar, 5 μm.

D. Red and green pixels overlap fraction (above) representing the co-localization of EGFR with the recycling marker Tf; green, red and far red pixels overlap fraction (below) representing the co-localization of EGFR, phosphorylated EGFR, and the recycling marker Tf in T47D stimulated for 40 min. Values represent the median ± SD of at least 3 independent experiments. Representative pictures are shown in C and Appendix Figure S6C. *, p value<0.005 (Student's t-test).

E. Co-localization of FGFR2 (red), EGFR (green), and the recycling marker Tf (blue) in T47D depleted of EGFR by siRNA followed by transfection with wt or T693A and stimulated or not with either FGF10 or TGFα for the indicated time periods. Scale bar, 5 μm.

F. Red and green pixels overlap fraction representing the co-localization of FGFR2 with EGFR; far red and green pixels overlap fraction representing the co-localization of EGFR with the recycling marker Tf; red and far red pixels overlap fraction representing the co-localization of FGFR2 with the recycling marker Tf; green, red and far red pixels overlap fraction representing the co-localization of FGFR2, EGFR, and the recycling marker Tf in cells stimulated for 20, 40, or 60 min. with FGF10 or TGFα. Values represent the median ± SD of at least 3 independent experiments. Representative pictures are shown in E. *, p value<0.005 (Student's t-test).

G. Lysates from T47D depleted of EGFR by siRNA followed by transfection with siRNA resistant wt or T693A and stimulated or not with either FGF10 or TGFα for the indicated time periods were used for immunoprecipitation of FGFR2 and then immunoblotted with the indicated antibodies. The inputs are shown in Appendix Figure S6F.

H. The presence (total), internalization (internalized), and recycling (cell surface) of FGFR2 in T47D depleted of EGFR by siRNA followed by transfection with wt or T693A and stimulated with FGF10 for different time periods were quantified as described (Francavilla *et al.*, 2016) and in the section 'Quantification of the Recycling Assay". Briefly, we assessed approximately 100 cells per condition and expressed the results as the percentage of receptor-positive cells over total cells (corresponding to DAPI-stained nuclei) and referred to the values obtained at time zero. Values represent the median ± SD of N=3. *, p value<0.005 (Student's t-test).

Figure 6. EGFR_T693 Phosphorylation Controls CDK1 Phosphorylation

A. Experimental design of MS-based quantitative phosphoproteomics analysis of wt- and T693A-expressing T47D cells stimulated with FGF10 for 40 or 60 min.

B. Hierarchical clustering of the phosphorylated sites differentially quantified in wt- and T693A-expressing T47D stimulated or not with FGF10 for 40 or 60 min.. Four clusters for plasma membrane Response (PMR), Acquired Response (AR), Late Response (LR), and T693 Phosphorylation Dependent Response (PDR) are highlighted with black lines and color-coded on the right with blue, medium, or dark blue and yellow, respectively. The intensity of phosphorylated sites is presented on the logarithmic scale with intensity below and above the mean color-coded in blue and red, respectively.

C. KEGG pathways enriched in each cluster.

D. STRING-based and Cytoscape-visualized network of phosphorylated kinases color-coded based on clusters shown in Figure 6C. The border of known regulatory sites is coloured in burgundy. The shape depends on the known function of the regulatory site.

E, F Lysates from T47D (E) and BT20 (F) depleted of EGFR, transfected with wt or T693A, and stimulated or not with either FGF10 or TGFα for the indicated time intervals were immunoblotted with the indicated antibodies.

Figure 7. FGF10-induced Cell Cycle Progression Depends on EGFR_T693 Phosphorylation

A-D Percentage of EdU incorporation in T47D (A, C) or BT20 (B, D) depleted of EGFR or not, transfected with wt or T693A, and stimulated or not with FGF10 (A, B) or with TGFα (C, D) and pre-treated (C, D) or not (A, B) with FGF10 for 40 min. Values represent the median ± SD of N= 4. P value =<0.05 *, <0.01 **, <0.001*** (one-way ANOVA with Tukey test).

E. Relative invasion of wt- or T693A-transfected BT20 cells into fibronectin-supplemented collagen I was quantified as described in Material and Methods. Graph depicts mean ± S.E.M. of N=8. *P value=<0.05 (Student's t-test).

F. Representative images of E. Black indicates cells. Confocal depth is indicated between panels. Scale bar, 250 μm.

G. Model of reciprocal priming between FGFR and EGFR, based on this study.

Figure EV1: xxxx Magnification of panels from stimulated T47D cells depleted of EGFR and transfection with wt EGFR

Individual panels and merge of each magnified section of T47D depleted of EGFR by siRNA followed by transfection with wt EGFR and stimulated or not with either FGF10 or TGFα for the indicated time periods. Scale bars are indicated in the figure. Panels from Figure 5E are shown on the left for comparison

Figure EV2: xxxx Magnification of panels from stimulated T47D cells depleted of EGFR and transfection with the EGFR_T693A mutant

Individual panels and merge of each magnified section of T47D depleted of EGFR by siRNA followed by transfection with EGFR_T693A and stimulated or not with either FGF10 or TGFα for the indicated time periods. Scale bars are indicated in the figure. Panels from Figure 5E are shown on the left for comparison

Figure EV3. xxxx Table summarizing the main findings of this study

Summary table of key observations made in this study, a brief description of the conditions these observations were made under, and the location of key results underpinning them.

REFERENCES

Babina IS, Turner NC (2017) Advances and challenges in targeting FGFR signalling in cancer. *Nat Rev Cancer* 17: 318-332

Barrow-McGee R, Kermorgant S (2014) Met endosomal signalling: in the right place, at the right time. *Int J Biochem Cell Biol* 49: 69-74

Baumdick M, Bruggemann Y, Schmick M, Xouri G, Sabet O, Davis L, Chin JW, Bastiaens PI (2015) EGF-dependent re-routing of vesicular recycling switches spontaneous phosphorylation suppression to EGFR signalling. *Elife* 4

Bergeron JJ, Di Guglielmo GM, Dahan S, Dominguez M, Posner BI (2016) Spatial and Temporal Regulation of Receptor Tyrosine Kinase Activation and Intracellular Signal Transduction. *Annu Rev Biochem* 85: 573-597

Bludau I, Aebersold R (2020) Proteomic and interactomic insights into the molecular basis of cell functional diversity. *Nat Rev Mol Cell Biol* 21: 327-340

Bolstad BM, Irizarry RA, Astrand M, Speed TP (2003) A comparison of normalization methods for high density oligonucleotide array data based on variance and bias. *Bioinformatics* 19: 185-193

Budick-Harmelin N, Miaczynska M (2018) Integration of the Endocytic System into the Network of Cellular Functions. *Prog Mol Subcell Biol* 57: 39-63

Butti R, Das S, Gunasekaran VP, Yadav AS, Kumar D, Kundu GC (2018) Receptor tyrosine kinases (RTKs) in breast cancer: signalling, therapeutic implications and challenges. *Mol Cancer* 17: 34

Cao X (2016) Self-regulation and cross-regulation of pattern-recognition receptor signalling in health and disease. *Nat Rev Immunol* 16: 35-50

Caswell P, Norman J (2008) Endocytic transport of integrins during cell migration and invasion. *Trends Cell Biol* 18: 257-263

Ceresa BP, Peterson JL (2014) Cell and molecular biology of epidermal growth factor receptor. *Int Rev Cell Mol Biol* 313: 145-178

Cheng Y, Tian H (2017) Current Development Status of MEK Inhibitors. *Molecules* 22

Clayton NS, Grose RP (2018) Emerging Roles of Fibroblast Growth Factor 10 in Cancer. *Front Genet* 9: 499

Collinet C, Stoter M, Bradshaw CR, Samusik N, Rink JC, Kenski D, Habermann B, Buchholz F, Henschel R, Mueller MS *et al* (2010) Systems survey of endocytosis by multiparametric image analysis. *Nature* 464: 243-249

Costes SV, Daelemans D, Cho EH, Dobbin Z, Pavlakis G, Lockett S (2004) Automatic and quantitative measurement of protein-protein colocalization in live cells. *Biophys J* 86: 3993-4003

Coulonval K, Kooken H, Roger PP (2011) Coupling of T161 and T14 phosphorylations protects cyclin B-CDK1 from premature activation. *Mol Biol Cell* 22: 3971-3985

Cox J, Hein MY, Luber CA, Paron I, Nagaraj N, Mann M (2014) Accurate proteome-wide label-free quantification by delayed normalization and maximal peptide ratio extraction, termed MaxLFQ. *Molecular & cellular proteomics : MCP* 13: 2513-2526

Cox J, Mann M (2008) MaxQuant enables high peptide identification rates, individualized p.p.b.-range mass accuracies and proteome-wide protein quantification. *Nat Biotechnol* 26: 1367-1372

Cox J, Neuhauser N, Michalski A, Scheltema RA, Olsen JV, Mann M (2011) Andromeda: a peptide search engine integrated into the MaxQuant environment. *J Proteome Res* 10: 1794-1805

Crupi MJF, Maritan SM, Reyes-Alvarez E, Lian EY, Hyndman BD, Rekab AN, Moodley S, Antonescu CN, Mulligan LM (2020) GGA3-mediated recycling of the RET receptor tyrosine kinase contributes to cell migration and invasion. *Oncogene* 39: 1361-1377

Doll S, Gnad F, Mann M (2019) The Case for Proteomics and Phospho-Proteomics in Personalized Cancer Medicine. *Proteomics Clin Appl* 13: e1800113

Du Z, Lovly CM (2018) Mechanisms of receptor tyrosine kinase activation in cancer. *Mol Cancer* 17: 58

Emami H, Vucic E, Subramanian S, Abdelbaky A, Fayad ZA, Du S, Roth E, Ballantyne CM, Mohler ER, Farkouh ME *et al* (2015) The effect of BMS-582949, a P38 mitogen-activated protein kinase (P38 MAPK) inhibitor on arterial inflammation: a multicenter FDG-PET trial. *Atherosclerosis* 240: 490-496

Eyre R, Alferez DG, Spence K, Kamal M, Shaw FL, Simoes BM, Santiago-Gomez A, Sarmiento-Castro A, Bramley M, Absar M *et al* (2016) Patient-derived Mammosphere and Xenograft Tumour Initiation Correlates with Progression to Metastasis. *Journal of mammary gland biology and neoplasia* 21: 99-109

Francavilla C, Cattaneo P, Berezin V, Bock E, Ami D, de Marco A, Christofori G, Cavallaro U (2009) The binding of NCAM to FGFR1 induces a specific cellular response mediated by receptor trafficking. *The Journal of cell biology* 187: 1101-1116

Francavilla C, Papetti M, Rigbolt KT, Pedersen AK, Sigurdsson JO, Cazzamali G, Karemore G, Blagoev B, Olsen JV (2016) Multilayered proteomics reveals molecular switches dictating ligand-dependent EGFR trafficking. *Nature structural & molecular biology* 23: 608-618

Francavilla C, Rigbolt KT, Emdal KB, Carraro G, Vernet E, Bekker-Jensen DB, Streicher W, Wikstrom M, Sundstrom M, Bellusci S *et al* (2013) Functional proteomics defines the molecular switch underlying FGF receptor trafficking and cellular outputs. *Molecular cell* 51: 707-722

Gan HK, Walker F, Burgess AW, Rigopoulos A, Scott AM, Johns TG (2007) The epidermal growth factor receptor (EGFR) tyrosine kinase inhibitor AG1478 increases the formation of inactive untethered EGFR dimers. Implications for combination therapy with monoclonal antibody 806. *The Journal of biological chemistry* 282: 2840-2850

Gillingham AK, Bertram J, Begum F, Munro S (2019) In vivo identification of GTPase interactors by mitochondrial relocalization and proximity biotinylation. *Elife* 8

Goh LK, Sorkin A (2013) Endocytosis of receptor tyrosine kinases. *Cold Spring Harb Perspect Biol* 5: a017459

Gut G, Herrmann MD, Pelkmans L (2018) Multiplexed protein maps link subcellular organization to cellular states. *Science* 361

Han Y, Caday CG, Nanda A, Cavenee WK, Huang HJ (1996) Tyrphostin AG 1478 preferentially inhibits human glioma cells expressing truncated rather than wild-type epidermal growth factor receptors. *Cancer research* 56: 3859-3861

Hanker AB, Garrett JT, Estrada MV, Moore PD, Ericsson PG, Koch JP, Langley E, Singh S, Kim PS, Frampton GM *et al* (2017) HER2-Overexpressing Breast Cancers Amplify FGFR Signalling upon Acquisition of Resistance to Dual Therapeutic Blockade of HER2. *Clin Cancer Res* 23: 4323-4334

Harbeck N, Penault-Llorca F, Cortes J, Gnant M, Houssami N, Poortmans P, Ruddy K, Tsang J, Cardoso F (2019) Breast cancer. *Nat Rev Dis Primers* 5: 66

Haugsten EM, Sorensen V, Brech A, Olsnes S, Wesche J (2005) Different intracellular trafficking of FGF1 endocytosed by the four homologous FGF receptors. *J Cell Sci* 118: 3869-3881

Heisermann GJ, Wiley HS, Walsh BJ, Ingraham HA, Fiol CJ, Gill GN (1990) Mutational removal of the Thr669 and Ser671 phosphorylation sites alters substrate specificity and ligand-induced internalization of the epidermal growth factor receptor. *The Journal of biological chemistry* 265: 12820-12827

Huang KL, Li S, Mertins P, Cao S, Gunawardena HP, Ruggles KV, Mani DR, Clauser KR, Tanioka M, Usary J *et al* (2017) Proteogenomic integration reveals therapeutic targets in breast cancer xenografts. *Nat Commun* 8: 14864

Huang PH (2012) Phosphoproteomic studies of receptor tyrosine kinases: future perspectives. *Mol Biosyst* 8: 1100-1107

Issa A, Gill JW, Heideman MR, Sahin O, Wiemann S, Dey JH, Hynes NE (2013) Combinatorial targeting of FGF and ErbB receptors blocks growth and metastatic spread of breast cancer models. *Breast Cancer Res* 15: R8

Kobayashi Y, Lim SO, Yamaguchi H (2019) Oncogenic signalling pathways associated with immune evasion and resistance to immune checkpoint inhibitors in cancer. *Semin Cancer Biol*

Lanzetti L, Di Fiore PP (2017) Behind the Scenes: Endo/Exocytosis in the Acquisition of Metastatic Traits. *Cancer research* 77: 1813-1817

Lemmon MA, Schlessinger J (2010) Cell signalling by receptor tyrosine kinases. *Cell* 141: 1117-1134

Liao Y, Wang J, Jaehnig EJ, Shi Z, Zhang B (2019) WebGestalt 2019: gene set analysis toolkit with revamped UIs and APIs. *Nucleic Acids Res* 47: W199-W205

Liberali P, Snijder B, Pelkmans L (2014) A hierarchical map of regulatory genetic interactions in membrane trafficking. *Cell* 157: 1473-1487

Lobingier BT, Huttenhain R, Eichel K, Miller KB, Ting AY, von Zastrow M, Krogan NJ (2017) An Approach to Spatiotemporally Resolve Protein Interaction Networks in Living Cells. *Cell* 169: 350-360 e312

Lundby A, Franciosa G, Emdal KB, Refsgaard JC, Gnosa SP, Bekker-Jensen DB, Secher A, Maurya SR, Paul I, Mendez BL *et al* (2019) Oncogenic Mutations Rewire Signalling Pathways by Switching Protein Recruitment to Phosphotyrosine Sites. *Cell* 179: 543-560 e526

Maennling AE, Tur MK, Niebert M, Klockenbring T, Zeppernick F, Gattenlohner S, Meinhold-Heerlein I, Hussain AF (2019) Molecular Targeting Therapy against EGFR Family in Breast Cancer: Progress and Future Potentials. *Cancers (Basel)* 11

Manders EM, Hoebe R, Strackee J, Vossepoel AM, Aten JA (1996) Largest contour segmentation: a tool for the localization of spots in confocal images. *Cytometry* 23: 15-21

McQuin C, Goodman A, Chernyshev V, Kamentsky L, Cimini BA, Karhohs KW, Doan M, Ding L, Rafelski SM, Thirstrup D *et al* (2018) CellProfiler 3.0: Next-generation image processing for biology. *PLoS Biol* 16: e2005970

Mellman I, Yarden Y (2013) Endocytosis and cancer. *Cold Spring Harb Perspect Biol* 5: a016949

Mertins P, Mani DR, Ruggles KV, Gillette MA, Clauser KR, Wang P, Wang X, Qiao JW, Cao S, Petralia F *et al* (2016) Proteogenomics connects somatic mutations to signalling in breast cancer. *Nature* 534: 55-62

Navid S, Fan C, P OF-V, Generali D, Li Y (2020) The Fibroblast Growth Factor Receptors in Breast Cancer: from Oncogenesis to Better Treatments. *Int J Mol Sci* 21

Neve RM, Chin K, Fridlyand J, Yeh J, Baehner FL, Fevr T, Clark L, Bayani N, Coppe JP, Tong F *et al* (2006) A collection of breast cancer cell lines for the study of functionally distinct cancer subtypes. *Cancer Cell* 10: 515-527

Nguyen LK, Kholodenko BN (2016) Feedback regulation in cell signalling: Lessons for cancer therapeutics. *Semin Cell Dev Biol* 50: 85-94

Olsen JV, Blagoev B, Gnad F, Macek B, Kumar C, Mortensen P, Mann M (2006) Global, in vivo, and site-specific phosphorylation dynamics in signalling networks. *Cell* 127: 635-648

Ornitz DM, Itoh N (2015) The Fibroblast Growth Factor signalling pathway. *Wiley Interdiscip Rev Dev Biol* 4: 215-266

Pardo OE, Latigo J, Jeffery RE, Nye E, Poulsom R, Spencer-Dene B, Lemoine NR, Stamp GW, Aboagye EO, Seckl MJ (2009) The fibroblast growth factor receptor inhibitor PD173074 blocks small cell lung cancer growth in vitro and in vivo. *Cancer research* 69: 8645-8651

Perez-Riverol Y, Csordas A, Bai J, Bernal-Llinares M, Hewapathirana S, Kundu DJ, Inuganti A, Griss J, Mayer G, Eisenacher M *et al* (2019) The PRIDE database and related tools and resources in 2019: improving support for quantification data. *Nucleic Acids Res* 47: D442-D450

Pletscher-Frankild S, Palleja A, Tsafou K, Binder JX, Jensen LJ (2015) DISEASES: text mining and data integration of disease-gene associations. *Methods* 74: 83-89

Porebska N, Latko M, Kucinska M, Zakrzewska M, Otlewski J, Opalinski L (2018) Targeting Cellular Trafficking of Fibroblast Growth Factor Receptors as a Strategy for Selective Cancer Treatment. *J Clin Med* 8

Sachs N, de Ligt J, Kopper O, Gogola E, Bounova G, Weeber F, Balgobind AV, Wind K, Gracanin A, Begthel H *et al* (2018) A Living Biobank of Breast Cancer Organoids Captures Disease Heterogeneity. *Cell* 172: 373-386 e310

Santiago-Gomez A, Kedward T, Simoes BM, Dragoni I, NicAmhlaoibh R, Trivier E, Sabin V, Gee JM, Sims AH, Howell SJ *et al* (2019) PAK4 regulates stemness and progression in endocrine resistant ER-positive metastatic breast cancer. *Cancer Lett* 458: 66-75

Schindelin J, Arganda-Carreras I, Frise E, Kaynig V, Longair M, Pietzsch T, Preibisch S, Rueden C, Saalfeld S, Schmid B *et al* (2012) Fiji: an open-source platform for biological-image analysis. *Nat Methods* 9: 676-682

Schmid SL (2017) Reciprocal regulation of signalling and endocytosis: Implications for the evolving cancer cell. *The Journal of cell biology* 216: 2623-2632

Shannon P, Markiel A, Ozier O, Baliga NS, Wang JT, Ramage D, Amin N, Schwikowski B, Ideker T (2003) Cytoscape: a software environment for integrated models of biomolecular interaction networks. *Genome Res* 13: 2498-2504

Sharrocks AD (2006) Cell cycle: sustained ERK signalling represses the inhibitors. *Curr Biol* 16: R540-542

Singhirunnusorn P, Ueno Y, Matsuo M, Suzuki S, Saiki I, Sakurai H (2007) Transient suppression of ligand-mediated activation of epidermal growth factor receptor by tumor necrosis factor-alpha through the TAK1-p38 signalling pathway. *The Journal of biological chemistry* 282: 12698-12706

Stallaert W, Bruggemann Y, Sabet O, Baak L, Gattiglio M, Bastiaens PIH (2018) Contact inhibitory Eph signalling suppresses EGF-promoted cell migration by decoupling EGFR activity from vesicular recycling. *Sci Signal* 11

Szklarczyk D, Gable AL, Lyon D, Junge A, Wyder S, Huerta-Cepas J, Simonovic M, Doncheva NT, Morris JH, Bork P *et al* (2019) STRING v11: protein-protein association networks with increased coverage, supporting functional discovery in genome-wide experimental datasets. *Nucleic Acids Res* 47: D607-D613

Tan AC, Vyse S, Huang PH (2017) Exploiting receptor tyrosine kinase co-activation for cancer therapy. *Drug Discov Today* 22: 72-84

Tate JG, Bamford S, Jubb HC, Sondka Z, Beare DM, Bindal N, Boutselakis H, Cole CG, Creatore C, Dawson E *et al* (2019) COSMIC: the Catalogue Of Somatic Mutations In Cancer. *Nucleic Acids Res* 47: D941-D947

Tomas A, Vaughan SO, Burgoyne T, Sorkin A, Hartley JA, Hochhauser D, Futter CE (2015) WASH and Tsg101/ALIX-dependent diversion of stress-internalized EGFR from the canonical endocytic pathway. *Nat Commun* 6: 7324

Tyanova S, Cox J (2018) Perseus: A Bioinformatics Platform for Integrative Analysis of Proteomics Data in Cancer Research. *Methods Mol Biol* 1711: 133-148

Uhlitz F, Sieber A, Wyler E, Fritsche-Guenther R, Meisig J, Landthaler M, Klinger B, Bluthgen N (2017) An immediate-late gene expression module decodes ERK signal duration. *Molecular systems biology* 13: 944

Watson J, Francavilla C (2018) Regulation of FGF10 Signalling in Development and Disease. *Front Genet* 9: 500

Weber F, Fukino K, Sawada T, Williams N, Sweet K, Brena RM, Plass C, Caldes T, Mutter GL, Villalona-Calero MA *et al* (2005) Variability in organ-specific EGFR mutational spectra in tumour epithelium and stroma may be the biological basis for differential responses to tyrosine kinase inhibitors. *Br J Cancer* 92: 1922-1926

Winograd-Katz SE, Levitzki A (2006) Cisplatin induces PKB/Akt activation and p38(MAPK) phosphorylation of the EGF receptor. *Oncogene* 25: 7381-7390

Wintheiser GA, Silberstein P (2020) Physiology, Tyrosine Kinase Receptors. In: *StatPearls*, Treasure Island (FL)

Wittkowski KM, Dadurian C, Seybold MP, Kim HS, Hoshino A, Lyden D (2018) Complex polymorphisms in endocytosis genes suggest alpha-cyclodextrin as a treatment for breast cancer. *PLoS One* 13: e0199012

Wu X, Zahari MS, Renuse S, Sahasrabuddhe NA, Chaerkady R, Kim MS, Fackler MJ, Stampfer M, Gabrielson E, Sukumar S *et al* (2018) Quantitative phosphoproteomic analysis reveals reciprocal activation of receptor tyrosine kinases between cancer epithelial cells and stromal fibroblasts. *Clin Proteomics* 15: 21

Yaffe MB (2019) Why geneticists stole cancer research even though cancer is primarily a signalling disease. *Sci Signal* 12

Zakrzewska M, Haugsten EM, Nadratowska-Wesolowska B, Oppelt A, Hausott B, Jin Y, Otlewski J, Wesche J, Wiedlocha A (2013) ERK-mediated phosphorylation of fibroblast growth factor receptor 1 on Ser777 inhibits signalling. *Sci Signal* 6: ra11

Zinkle A, Mohammadi M (2019) Structural Biology of the FGF7 Subfamily. *Front Genet* 10: 102

Zwang Y, Yarden Y (2006) p38 MAP kinase mediates stress-induced internalization of EGFR: implications for cancer chemotherapy. *EMBO J* 25: 4195-4206

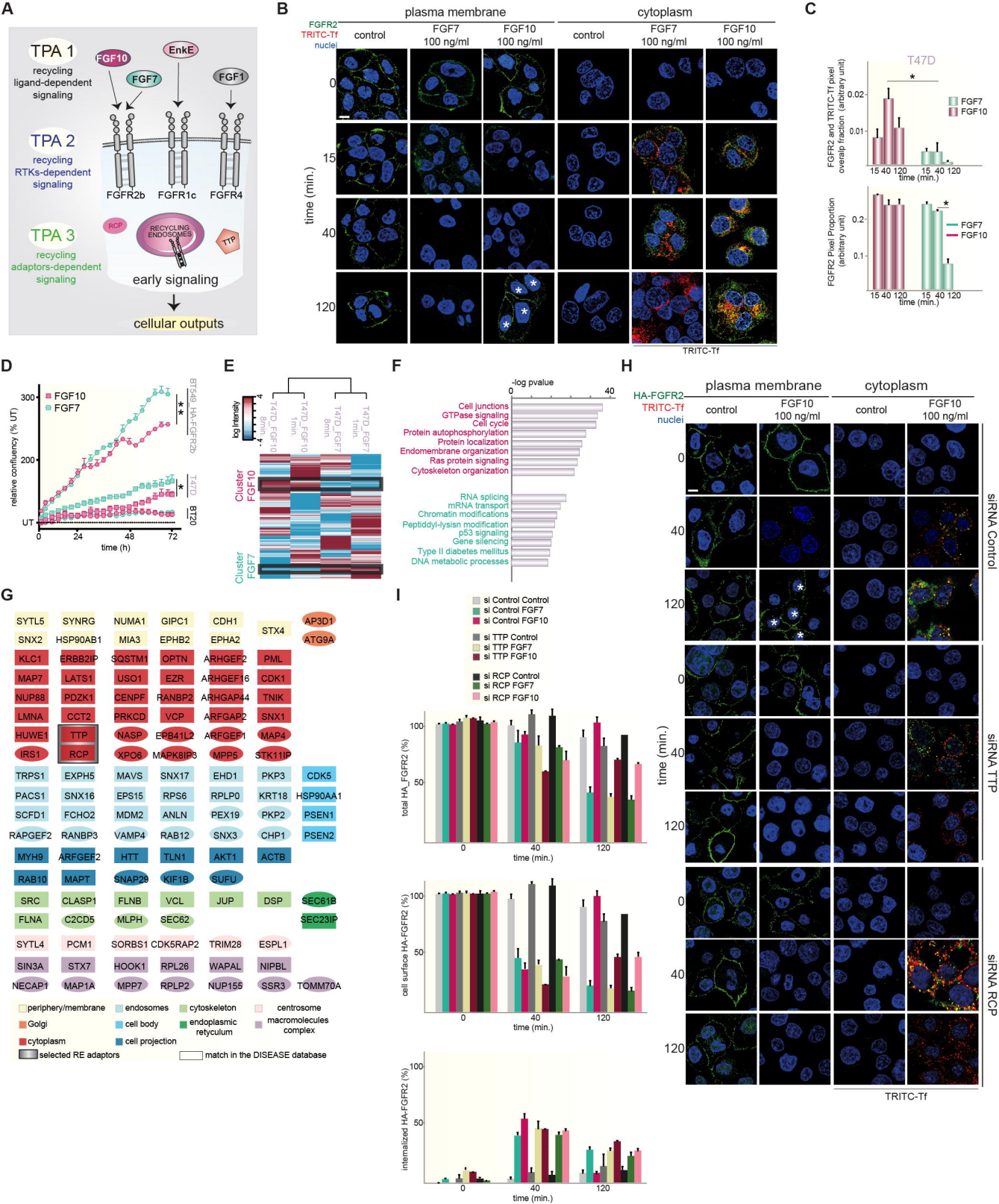
A
TPA 1
recycling ligand-dependent signaling
FGF10
EnkE
FGF7
FGF1
TPA 2
recycling RTKs-dependent signaling
FGFR2b
FGFR1c
FGFR4
TPA 3
recycling adaptors-dependent signaling
RCP
RECYCLING ENDOSOMES
TTP
early signaling
cellular outputs
B
plasma membrane
cytoplasm
FGFR2
TRITC-Tf
nuclei
control
FGF7 100 ng/ml
FGF10 100 ng/ml
time (min.)
TRITC-Tf
C
T47D
FGF2 and TRITC-Tf pixel overalp fraction (arbitrary unit)
FGF2 Pixel Proportion (arbitrary unit)
FGF7
FGF10
time (min.)
D
FGF10
FGF7
relative confluency (% UT)
time (h)
BT549_HA-FGFR2b
T47D
BT20
E
log Intensity
Cluster FGF10
Cluster FGF7
F
-log pvalue
Cell junctions
GTPase signaling
Cell cycle
Protein autophosphorylation
Protein localization
Endomembrane organization
Ras protein signaling
Cytoskeleton organization
RNA splicing
mRNA transport
Chromatin modifications
Peptidyl-lysisn modification
p53 signaling
Gene silencing
Type II diabetes mellitus
DNA metabolic processes
G
SYTL5 SYNRG NUMA1 GIPC1 CDH1 STX4 AP3D1
SNX2 HSP90AB1 MIA3 EPHB2 EPHA2 ATG9A
KLC1 ERBB2IP SQSTM1 OPTN ARHGEF2 PML
MAP7 LATS1 USO1 EZR ARHGEF16 CDK1
NUP88 PDZK1 CENPF RANBP2 ARHGAP44 TNIK
LMNA CCT2 PRKCD VCP ARFGAP2 SNX1
HUWE1 TTP NASP EPB41L2 ARFGEF1 MAP4
IRS1 RCP XPO6 MAPK8IP3 MPP5 STK11IP
TRPS1 EXPH5 MAVS SNX17 EHD1 PKP3 CDK5
PACS1 SNX16 EPS15 RPS6 RPLP0 KRT18 HSP90AA1
SCFD1 FCHO2 MDM2 ANLN PEX19 PKP2 PSEN1
RAPGEF2 RANBP3 VAMP4 RAB12 SNX3 CHP1 PSEN2
MYH9 ARFGEF2 HTT TLN1 AKT1 ACTB
RAB10 MAPT SNAP29 KIF1B SUFU
SRC CLASP1 FLNB VCL JUP DSP SEC61B
FLNA C2CD5 MLPH SEC62 SEC23IP
SYTL4 PCM1 SORBS1 CDK5RAP2 TRIM28 ESPL1
SIN3A STX7 HOOK1 RPL26 WAPAL NIPBL
NECAP1 MAP1A MPP7 RPLP2 NUP155 SSR3 TOMM70A
periphery/membrane
endosomes
cytoskeleton
centrosome
Golgi
cell body
endoplasmic retyculum
macromolecules complex
cytoplasm
cell projection
selected RE adaptors
match in the DISEASE database
I
si Control Control
si Control FGF7
si Control FGF10
si TTP Control
si TTP FGF7
si TTP FGF10
si RCP Control
si RCP FGF7
si RCP FGF10
total HA_FGFR2 (%)
cell surface HA-FGFR2 (%)
internalized HA-FGFR2 (%)
time (min.)
H
HA-FGFR2
TRITC-Tf
nuclei
plasma membrane
cytoplasm
control
FGF10 100 ng/ml
time (min.)
siRNA Control
siRNA TTP
siRNA RCP
TRITC-Tf

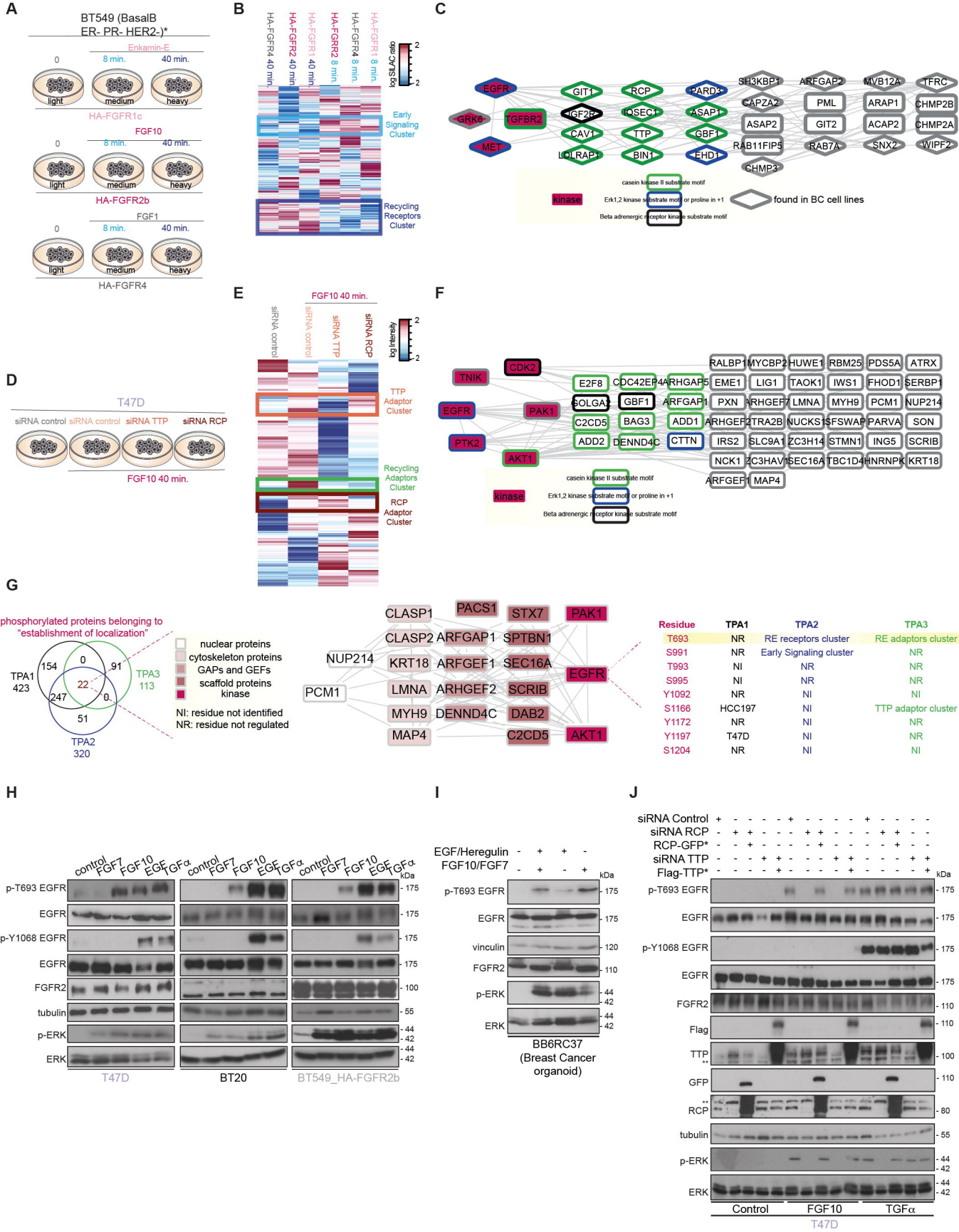
A
BT549 (BasalB ER- PR- HER2-)*
Enkamin-E
0
8 min.
40 min.
light
medium
heavy
HA-FGFR1c
FGF10
HA-FGFR2b
FGF1
HA-FGFR4
B
HA-FGFR4 40 min.
HA-FGFR2 40 min.
HA-FGFR1 40 min.
HA-FGFR2 8 min.
HA-FGFR4 8 min.
HA-FGFR1 8 min.
log SILAC ratio
Early Signaling Cluster
Recycling Receptors Cluster
C
EGFR
GRK6
MET
TGFBR2
IGF2R
GIT1
CAV1
LDLRAP1
RCP
OSEC1
TTP
BIN1
PARD3
ASAP1
GBF1
EHD1
SH3KBP1
CAPZA2
ASAP2
RAB11FIP5
CHMP3
ARFGAP2
PML
GIT2
RAB7A
MVB12A
ARAP1
ACAP2
SNX2
TFRC
CHMP2B
CHMP2A
WIPF2
kinase
casein kinase II substrate motif
Erk1,2 kinase substrate motif or proline in +1
Beta adrenergic receptor kinase substrate motif
found in BC cell lines
D
T47D
siRNA control
siRNA control
siRNA TTP
siRNA RCP
FGF10 40 min.
E
FGF10 40 min.
siRNA control
siRNA control
siRNA TTP
siRNA RCP
log Intensity
TTP Adaptor Cluster
Recycling Adaptors Cluster
RCP Adaptor Cluster
F
TNIK
CDK2
EGFR
PAK1
PTK2
AKT1
E2F8
CDC42EP4
RHGAP5
SOLGA1
GBF1
ARFGAP1
C2CD5
BAG3
ADD1
ADD2
DENND4C
CTTN
RALBP1
MYCBP2
HUWE1
RBM25
PDS5A
ATRX
EME1
LIG1
TAOK1
IWS1
FHOD1
SERBP1
PXN
ARHGEF7
LMNA
MYH9
PCM1
NUP214
ARHGEF2
TRA2B
NUCKS1
SFSWAP
PARVA
SON
IRS2
SLC9A1
ZC3H14
STMN1
ING5
SCRIB
NCK1
ZC3HAV1
SEC16A
TBC1D4
HNRNPK
KRT18
ARFGEF1
MAP4
kinase
casein kinase II substrate motif
Erk1,2 kinase substrate motif or proline in +1
Beta adrenergic receptor kinase substrate motif
G
phosphorylated proteins belonging to "establishment of localization"
TPA1 423
TPA3 113
TPA2 320
154
0
91
22
247
0
51
nuclear proteins
cytoskeleton proteins
GAPs and GEFs
scaffold proteins
kinase
NI: residue not identified
NR: residue not regulated
CLASP1
CLASP2
NUP214
PCM1
PACS1
ARFGAP1
KRT18
ARFGEF1
LMNA
ARHGEF2
MYH9
DENND4C
MAP4
STX7
SPTBN1
SEC16A
SCRIB
DAB2
C2CD5
PAK1
EGFR
AKT1
Residue | TPA1 | TPA2 | TPA3
T693 | NR | RE receptors cluster | RE adaptors cluster
S991 | NR | Early Signaling cluster | NR
T993 | NI | NR | NR
S995 | NI | NR | NR
Y1092 | NR | NI | NI
S1166 | HCC197 | NI | TTP adaptor cluster
Y1172 | NR | NI | NR
Y1197 | T47D | NI | NR
S1204 | NR | NI | NI
H
control
FGF7
FGF10
EGF
TGFα
kDa
p-T693 EGFR
EGFR
p-Y1068 EGFR
EGFR
FGFR2
tubulin
p-ERK
ERK
175
175
175
175
100
55
44
42
44
42
T47D
BT20
BT549_HA-FGFR2b
I
EGF/Heregulin
FGF10/FGF7
kDa
p-T693 EGFR
EGFR
vinculin
FGFR2
p-ERK
ERK
175
175
120
110
44
42
44
42
BB6RC37 (Breast Cancer organoid)
J
siRNA Control
siRNA RCP
RCP-GFP*
siRNA TTP
Flag-TTP*
kDa
p-T693 EGFR
EGFR
p-Y1068 EGFR
EGFR
FGFR2
Flag
TTP
GFP
RCP
tubulin
p-ERK
ERK
175
175
175
175
110
110
100
110
80
55
44
42
44
42
Control
FGF10
TGFα
T47D

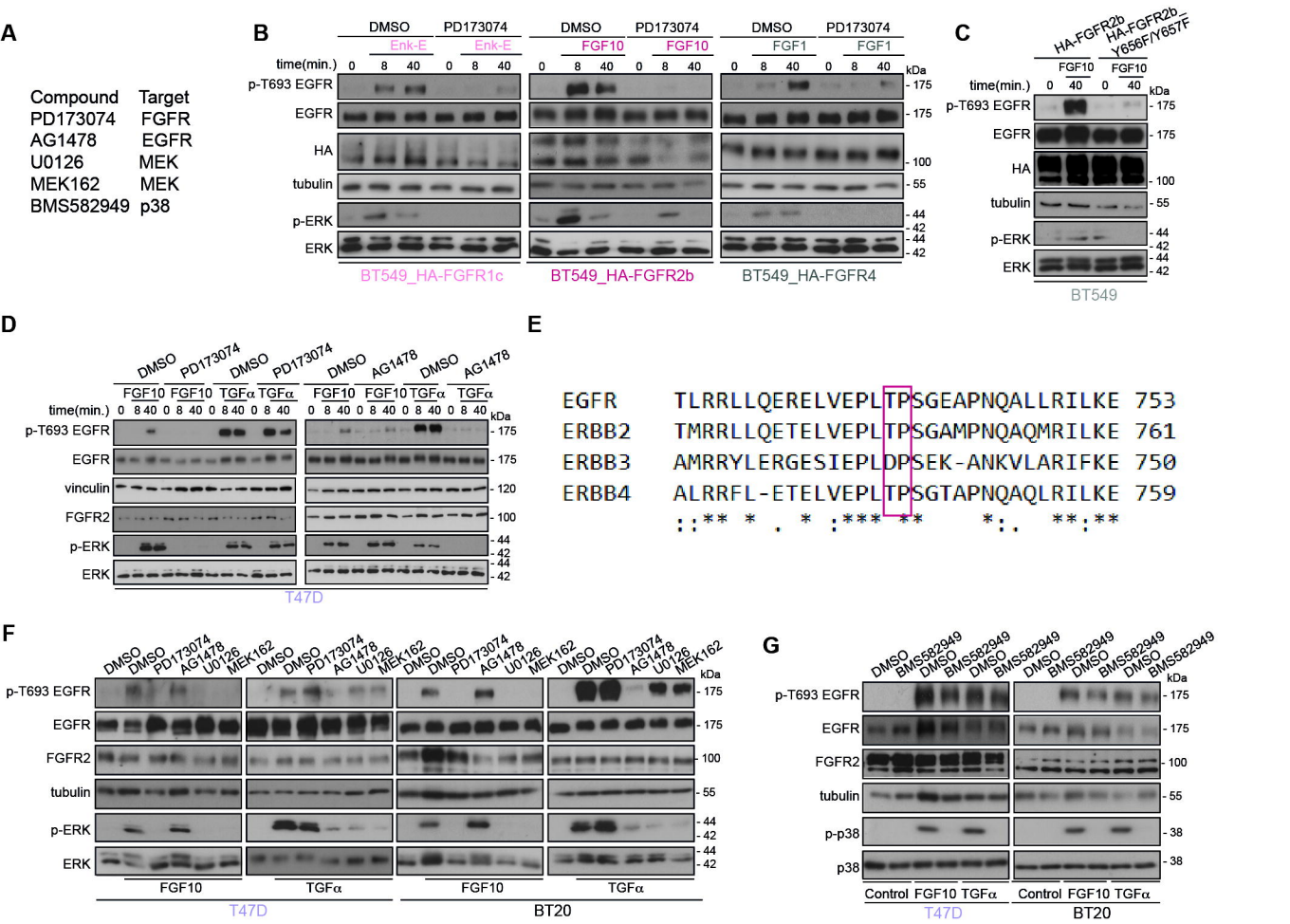
A
Compound Target
PD173074 FGFR
AG1478 EGFR
U0126 MEK
MEK162 MEK
BMS582949 p38
B
DMSO PD173074 DMSO PD173074 DMSO PD173074
Enk-E Enk-E FGF10 FGF10 FGF1 FGF1
time(min.) 0 8 40 0 8 40 0 8 40 0 8 40 0 8 40 0 8 40
kDa
p-T693 EGFR
EGFR
HA
tubulin
p-ERK
ERK
175
175
100
55
44
42
44
42
BT549_HA-FGFR1c
BT549_HA-FGFR2b
BT549_HA-FGFR4
C
HA-FGFR2b
HA-FGFR2b_Y656F/Y657F
FGF10 FGF10
time(min.) 0 40 0 40
kDa
p-T693 EGFR
EGFR
HA
tubulin
p-ERK
ERK
175
175
100
55
44
42
44
42
BT549
D
DMSO PD173074 DMSO PD173074 DMSO AG1478 DMSO AG1478
FGF10 FGF10 TGFα TGFα FGF10 FGF10 TGFα TGFα
time(min.) 0 8 40 0 8 40 0 8 40 0 8 40 0 8 40 0 8 40 0 8 40 0 8 40
kDa
p-T693 EGFR
EGFR
vinculin
FGFR2
p-ERK
ERK
175
175
120
100
44
42
44
42
T47D
E
EGFR TLRRLLQERELVEPLTPSGEAPNQALLRILKE 753
ERBB2 TMRRLLQETELVEPLTPSGAMPNQAQMRILKE 761
ERBB3 AMRRYLERGESIEPLDPSEK-ANKVLARIFKE 750
ERBB4 ALRRFL-ETELVEPLTPSGTAPNQAQLRILKE 759
::** * . * :*** ** *:. **:**
F
DMSO DMSO PD173074 AG1478 U0126 MEK162 DMSO DMSO PD173074 AG1478 U0126 MEK162 DMSO DMSO PD173074 AG1478 U0126 MEK162 DMSO DMSO PD173074 AG1478 U0126 MEK162
kDa
p-T693 EGFR
EGFR
FGFR2
tubulin
p-ERK
ERK
175
175
100
55
44
42
44
42
FGF10 TGFα FGF10 TGFα
T47D
BT20
G
DMSO BMS582949 DMSO BMS582949 DMSO BMS582949 DMSO BMS582949 DMSO BMS582949 DMSO BMS582949
kDa
p-T693 EGFR
EGFR
FGFR2
tubulin
p-p38
p38
175
175
100
55
38
38
Control FGF10 TGFα Control FGF10 TGFα
T47D
BT20

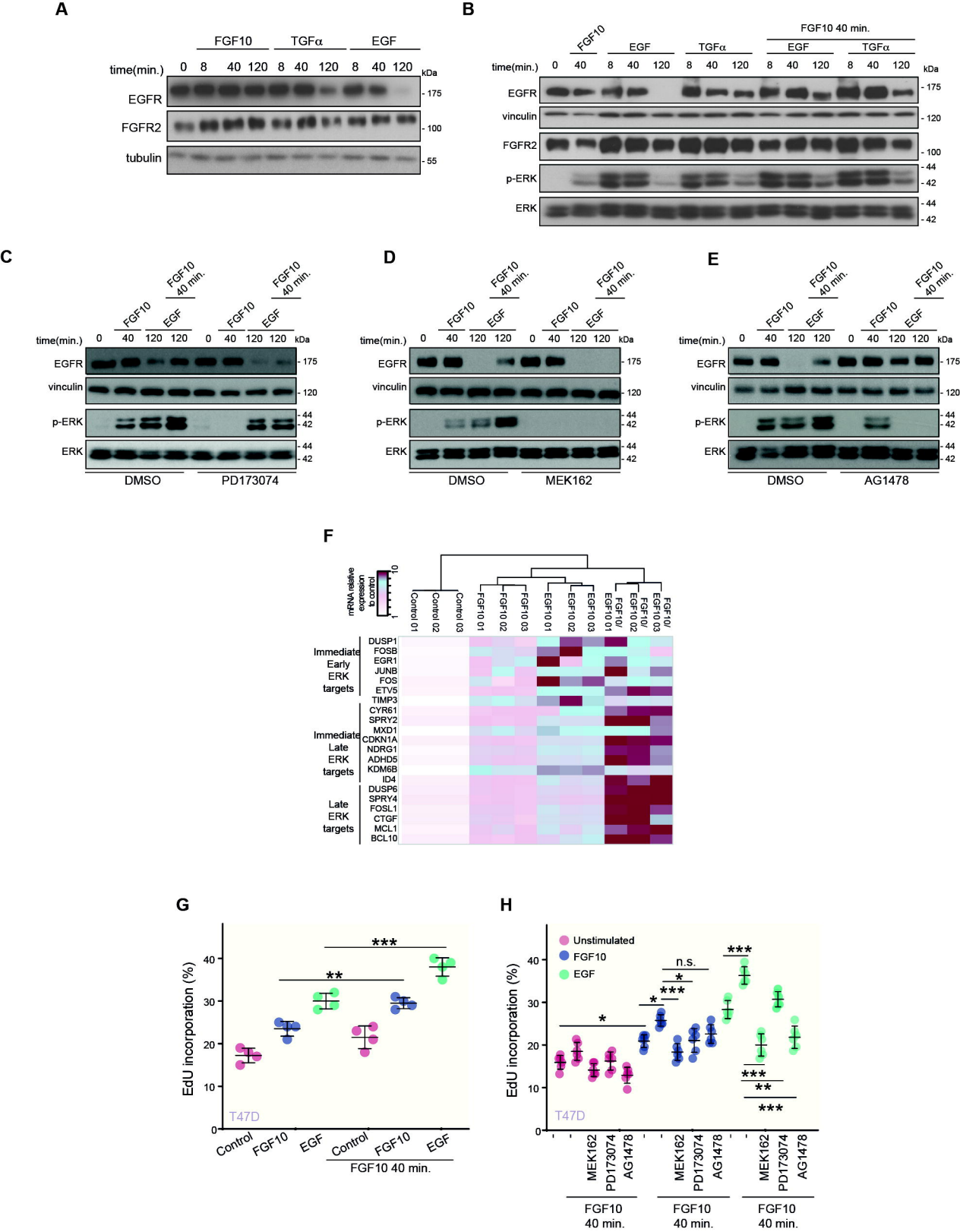
A
FGF10
TGFα
EGF
time(min.)
0 8 40 120 8 40 120 8 40 120
kDa
EGFR
FGFR2
tubulin
175
100
55
B
FGF10
EGF
TGFα
FGF10 40 min.
EGF
TGFα
time(min.)
0 40 8 40 120 8 40 120 8 40 120 8 40 120
EGFR
vinculin
FGFR2
p-ERK
ERK
175
120
100
44
42
C
FGF10
EGF
FGF10 40 min.
time(min.)
0 40 120 120 0 40 120 120
EGFR
vinculin
p-ERK
ERK
DMSO
PD173074
D
DMSO
MEK162
E
DMSO
AG1478
F
mRNA relative expression
Control 01
Control 02
Control 03
FGF10 01
FGF10 02
FGF10 03
EGF10 01
EGF10 02
EGF10 03
FGF10/ EGF10 01
FGF10/ EGF10 02
FGF10/ EGF10 03
Immediate Early ERK targets
DUSP1
FOSB
EGR1
JUNB
FOS
ETV5
TIMP3
Immediate Late ERK targets
CYR61
SPRY2
MXD1
CDKN1A
NDRG1
ADHD5
KDM6B
ID4
Late ERK targets
DUSP6
SPRY4
FOSL1
CTGF
MCL1
BCL10
G
EdU incorporation (%)
T47D
Control
FGF10
EGF
FGF10 40 min.
H
Unstimulated
FGF10
EGF
n.s.
MEK162
PD173074
AG1478
FGF10 40 min.

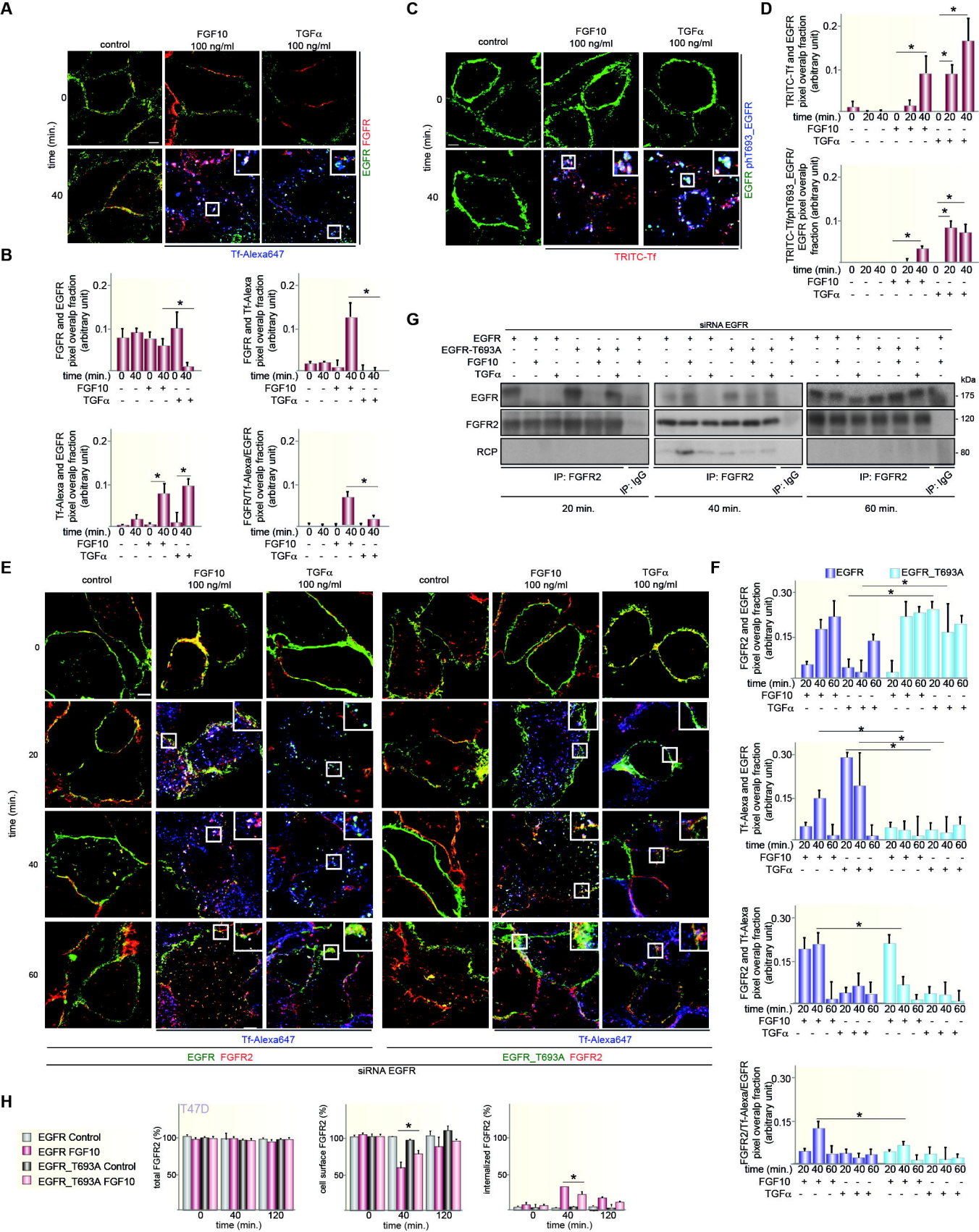
A
control
FGF10 100 ng/ml
TGFα 100 ng/ml
time (min.)
0
40
EGFR FGFR
Tf-Alexa647
B
FGFR and EGFR pixel overalp fraction (arbitrary unit)
FGFR and Tf-Alexa pixel overalp fraction (arbitrary unit)
Tf-Alexa and EGFR pixel overalp fraction (arbitrary unit)
FGFR/Tf-Alexa/EGFR pixel overalp fraction (arbitrary unit)
time (min.) 0 40 0 40 0 40
FGF10
TGFα
C
EGFR phT693_EGFR
TRITC-Tf
D
TRITC-Tf and EGFR pixel overalp fraction (arbitrary unit)
TRITC-Tf/phT693_EGFR/ EGFR pixel overalp fraction (arbitrary unit)
time (min.) 0 20 40 0 20 40 0 20 40
FGF10
TGFα
G
siRNA EGFR
EGFR
EGFR-T693A
FGF10
TGFα
kDa
175
120
80
EGFR
FGFR2
RCP
IP: FGFR2
IP: IgG
20 min.
40 min.
60 min.
E
control
FGF10 100 ng/ml
TGFα 100 ng/ml
time (min.)
0
20
40
60
Tf-Alexa647
EGFR FGFR2
EGFR_T693A FGFR2
siRNA EGFR
F
EGFR
EGFR_T693A
FGFR2 and EGFR pixel overalp fraction (arbitrary unit)
Tf-Alexa and EGFR pixel overalp fraction (arbitrary unit)
FGFR2 and Tf-Alexa pixel overalp fraction (arbitrary unit)
FGFR2/Tf-Alexa/EGFR pixel overalp fraction (arbitrary unit)
time (min.) 20 40 60 20 40 60 20 40 60 20 40 60
FGF10
TGFα
H
T47D
EGFR Control
EGFR FGF10
EGFR_T693A Control
EGFR_T693A FGF10
total FGFR2 (%)
cell surface FGFR2 (%)
internalized FGFR2 (%)
time (min.)

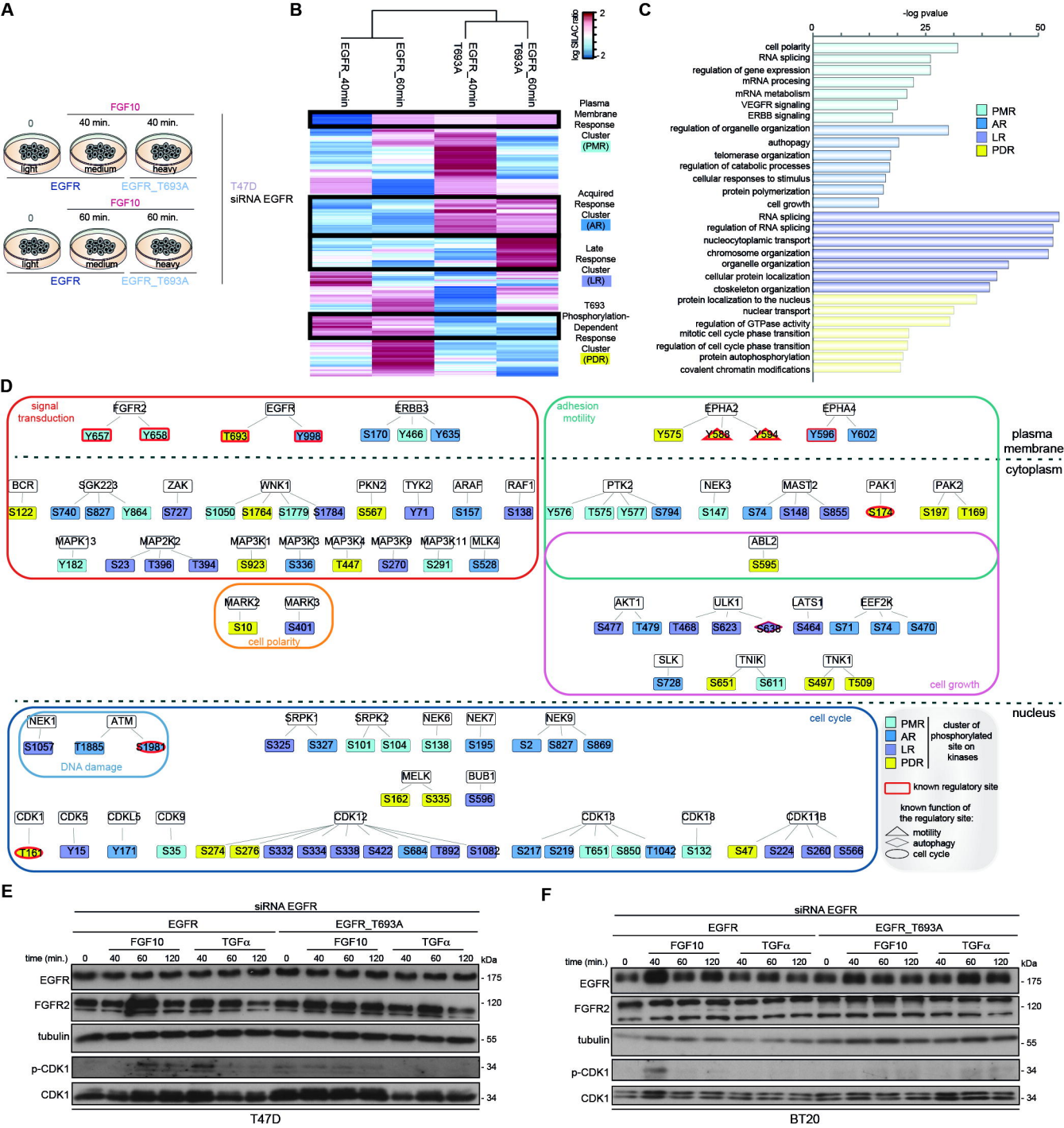
A
FGF10
0
40 min.
40 min.
light
medium
heavy
EGFR
EGFR_T693A
FGF10
0
60 min.
60 min.
light
medium
heavy
EGFR
EGFR_T693A
T47D
siRNA EGFR
B
EGFR_40min
EGFR_60min
EGFR_40min T693A
EGFR_60min T693A
log2(Ratio)
2
-2
Plasma Membrane Response Cluster (PMR)
Acquired Response Cluster (AR)
Late Response Cluster (LR)
T693 Phosphorylation-Dependent Response Cluster (PDR)
C
-log pvalue
0
25
50
cell polarity
RNA splicing
regulation of gene expression
mRNA procesing
mRNA metabolism
VEGFR signaling
ERBB signaling
regulation of organelle organization
authopagy
telomerase organization
regulation of catabolic processes
cellular responses to stimulus
protein polymerization
cell growth
RNA splicing
regulation of RNA splicing
nucleocytoplamic transport
chromosome organization
organelle organization
cellular protein localization
ctoskeleton organization
protein localization to the nucleus
nuclear transport
regulation of GTPase activity
mitotic cell cycle phase transition
regulation of cell cycle phase transition
protein autophosphorylation
covalent chromatin modifications
PMR
AR
LR
PDR
D
signal transduction
EGFR2
Y657
Y658
EGFR
T693
Y998
ERBB3
S170
Y466
Y635
adhesion motility
EPHA2
Y575
Y588
Y594
EPHA4
Y596
Y602
plasma membrane
cytoplasm
BCR
S122
SGK223
S740
S827
Y864
ZAK
S727
WNK1
S1050
S1764
S1779
S1784
PKN2
S567
TYK2
Y71
ARAF
S157
RAF1
S138
MAPK13
Y182
MAP2K2
S23
T396
T394
MAP3K1
S923
MAP3K3
S336
MAP3K4
T447
MAP3K9
S270
MAP3K11
S291
MLK4
S528
MARK2
S10
MARK3
S401
cell polarity
PTK2
Y576
T575
Y577
S794
NEK3
S147
MAST2
S74
S148
S855
PAK1
S174
PAK2
S197
T169
ABL2
S595
AKT1
S477
T479
T468
ULK1
S623
S638
LATS1
S464
EEF2K
S71
S74
S470
SLK
S728
TNIK
S651
S611
TNK1
S497
T509
cell growth
nucleus
NEK1
S1057
ATM
T1885
S1981
DNA damage
SRPK1
S325
S327
SRPK2
S101
S104
NEK6
S138
NEK7
S195
NEK9
S2
S827
S869
cell cycle
MELK
S162
S335
BUB1
S596
CDK1
T161
CDK5
Y15
CDKL5
Y171
CDK9
S35
CDK12
S274
S276
S332
S334
S338
S422
S684
T892
S1082
CDK13
S217
S219
T651
S850
T1042
CDK18
S132
CDK11B
S47
S224
S260
S566
PMR
AR
LR
PDR
cluster of phosphorylated site on kinases
known regulatory site
known function of the regulatory site:
motility
autophagy
cell cycle
E
siRNA EGFR
EGFR
EGFR_T693A
FGF10
TGFα
FGF10
TGFα
time (min.)
0
40
60
120
40
60
120
0
40
60
120
40
60
120
kDa
EGFR
FGFR2
tubulin
p-CDK1
CDK1
175
120
55
34
34
T47D
F
siRNA EGFR
EGFR
EGFR_T693A
FGF10
TGFα
FGF10
TGFα
time (min.)
0
40
60
120
40
60
120
0
40
60
120
40
60
120
kDa
EGFR
FGFR2
tubulin
p-CDK1
CDK1
175
120
55
34
34
BT20

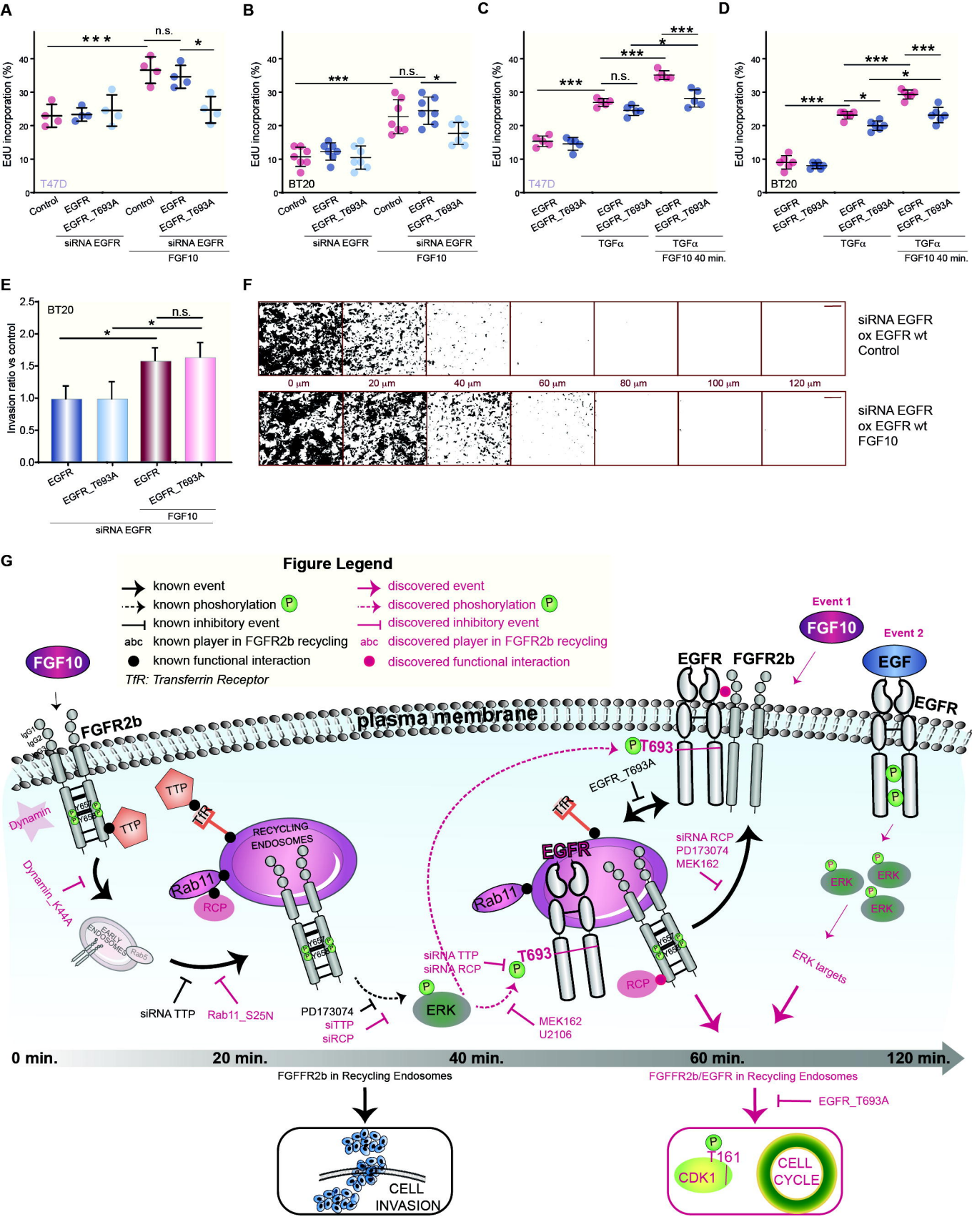
A
B
C
D
EdU incorporation (%)
T47D
BT20
Control
EGFR
EGFR_T693A
siRNA EGFR
FGF10
TGFα
FGF10 40 min.
n.s.
E
Invasion ratio vs control
F
0 µm
20 µm
40 µm
60 µm
80 µm
100 µm
120 µm
siRNA EGFR
ox EGFR wt
Control
FGF10
G
Figure Legend
known event
known phoshorylation
known inhibitory event
known player in FGFR2b recycling
known functional interaction
TfR: Transferrin Receptor
discovered event
discovered phoshorylation
discovered inhibitory event
discovered player in FGFR2b recycling
discovered functional interaction
Event 1
Event 2
FGF10
EGF
EGFR
FGFR2b
plasma membrane
IgG1
IgG2
Dynamin
Dynamin_K44A
TTP
TfR
RECYCLING ENDOSOMES
Rab11
RCP
EARLY ENDOSOMES
Rab5
siRNA TTP
Rab11_S25N
PD173074
siTTP
siRCP
ERK
T693
EGFR_T693A
siRNA RCP
PD173074
MEK162
siRNA TTP
siRNA RCP
MEK162
U2106
ERK targets
0 min.
20 min.
40 min.
60 min.
120 min.
FGFFR2b in Recycling Endosomes
FGFFR2b/EGFR in Recycling Endosomes
EGFR_T693A
CELL INVASION
T161
CDK1
CELL CYCLE